PRECISION CURRENT CONTROL FOR QUANTUM CASCADE LASERS AS FLIGHT CALIBRATION SOURCES

by

Stewart M. Hansen

A thesis submitted in partial fulfillment
of the requirements for the degree

of

MASTER OF SCIENCE

in

Electrical Engineering

Approved:

Dr. Doran Baker Major Professor	Dr. Donald Cripps Committee Member
Dr. Blake Crowther Committee Member	Dr. Mark R. McLellan Vice President for Research and Dean of the School of Graduate Studies

UTAH STATE UNIVERSITY
Logan, Utah

2014

Abstract

Precision Current Control for Quantum Cascade Lasers as Flight Calibration Sources

by

Stewart M. Hansen, Master of Science

Utah State University, 2014

Major Professor: Dr. Doran Baker
Department: Electrical and Computer Engineering

A space-grade-equivalent precision current controller for quantum cascade lasers (QCLs) is presented. This current controller design will enable constant wave (CW) or pulsed mode operation of QCL devices as calibration sources in a space environment. One major source of sensitivity in current controllers is temperature variation across the electronics board. This design integrates some methods used by Pacific Northwest National Laboratory (PNNL) to compensate for these sensitivites. An uncertainty analysis of the key components of the space-grade-equivialent current controller was performed to estimate changes in QCL output power due to a change of 1°C. The performed uncertainty analysis shows that the design has the capability to control the current to within the 0.1% output power stability goal with a change of ± 10°C in the precision current controller electronics.

(61 pages)

Public Abstract

Precision Current Control for Quantum Cascade Lasers as Flight Calibration Sources

by

Stewart M. Hansen, Master of Science

Utah State University, 2014

Major Professor: Dr. Doran Baker
Department: Electrical and Computer Engineering

The design of a precision current controller for quantum cascade lasers (QCLs) enables QCLs to be used for calibrating instruments in space-borne applications. This current controller design will enable constant wave (CW) or pulsed mode operation of QCL devices as calibration sources in a space environment. Any differences in the temperature between components of the current controller can result in an erroneous current through the QCL. This design will use previously demonstrated techniques from Pacific Northwest National Laboratory (PNNL) to minimize the effects of temperature changes on the desired current levels. A mathematical model is used to calculate what performance levels can be expected, and if the board can operate with a desired precision level of 0.1% of the desired power output of the QCL. This mathematical model shows the capability to control to the desired 0.1% output power stability with a change in the boards temperature of $\pm 10°$C.

Acknowledgments

I would like to thank Dr. Doran Baker, Dr. Blake Crowther, and Dr. Donald Cripps for their dedicated time and support in furthering the research for this thesis along with the Department of Energy for funding the project under contract number DE-NA0001740 making this research possible. I would also like to thank those at the Space Dynamics Laboratory who helped in mentoring and working on this research, in particular, Wally Gibbons, Bultu Hirpa, Alan Thurgood, Cory Harker, the machinists, and PCB technicians, along with the help from Pacific Northwest National Laboratory, in particular, Dr. Matthew Taubman, Dr. Bret Cannon, and Dr. Tanya Myers. I would also like to thank those at Utah State University who helped with any aspect of this project, in particular, Heidi Harper and Jill Ballard, along with H. Scott Hinton who gave access to his lab for this research.

Stewart M. Hansen

Contents

List of Tables

List of Figures

Chapter 1

Introduction

Optical remote sensing payloads on satellites are designed to make measurements of the incoming radiance. Since satellites operate outside the Earth's atmosphere as shown in Figure 1.1, this exposes them to the radiation of the space environment. Radiation can cause degradation in sensors and instruments as shown by examples from previous satellite flights [1]. To counteract degradation of instruments there needs to be a standard with which to compare the instruments' output. For example, if the sensor is designed to measure infrared radiation wavelengths then a source that emits the desired infrared radiation can be used to compare with the instrument's output. The source used for comparison is usually referred to as a calibration source.

Calibration sources are chosen based upon their known output characteristics, where the desired characteristics are determined by the application of the instrument and the environment of interest [2]. Signal changes can be due to detector changes or real changes in the remotely sensed object. Having a calibration source to characterize sensor response domains of interest helps relate what is being measured, as stated by Tansock et al calibration can be used to relate a sensor's output to "the true scene radiance" [3]. Calibration ensures that the output of the instrument is consistent with previous measurements and to ascertain the accuracy or precision of the instrument.

Recent studies at Pacific Northwest National Laboratories (PNNL) show promising results for the use of quantum cascade lasers (QCLs) as calibration sources [4]. A review of calibration sources and their operational properties will be discussed. For QCLs to be used as calibration sources a precision current controller is needed. The controller designed with help from Space Dynamics Laboratory (SDL) and PNNL will be discussed with focus on the flight precision current controller. Taking an uncertainty analysis of the design yields

promising results for precision current control for a QCL power output stability of at least 0.1%.

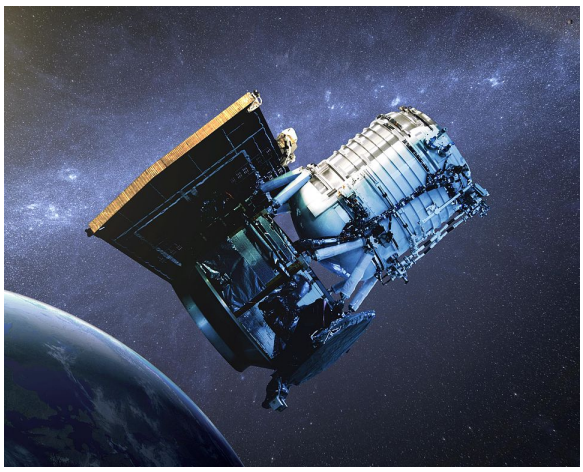

Fig. 1.1: NASA/SDL WISE satellite artist rendition (Wikipedia Commons).

Chapter 2

Calibration Sources

Calibration sources that are used on satellite systems are typically known as flight calibration sources. Sources that produce controlled electromagnetic radiation at ultraviolet (UV) to infrared (IR) wavelength can come in the forms of various light emitting devices. These calibration devices can be a blackbody, a light emitting diode, or a laser.

2.1 Blackbodies

Blackbodies are idealized physical surfaces that absorb all incident light [5]. Their radiation characteristics are calculated using fundamental laws of physics [6]. The radiation from the blackbody is emitted according to Planck's law, and changes with respect to the temperature of the body [5]. Blackbodies are ideal emitters in the sense that they emit the same or more energy at every frequency than other bodies will at the same temperature. A blackbody is also ideal because it is a diffuse emitter, so the energy is radiated isotropically or independent of direction. These blackbody sources come in different forms; the two main forms are lamp or cavity sources.

A lamp blackbody would be a filament type light source, in which the filament changes radiation spectrum according to its temperature. An example is a Stefan-Boltzmann lamp or tungsten lamp, where the temperature of the filament is affected by the ambient temperature and the electrical current in the filament [5, 7].

The key objective of a cavity blackbody design is to provide an isothermal emissivity-enhancing cavity which uses minimal power to maintain stable temperatures [8]. The aperture into the cavity should be small, and the coating inside the cavity should be a high emissivity surface, where emissivity is the ability to emit energy by radiation. Surrounding the exterior of the cavity, a temperature sensor and heater can be used to sense and control

the temperature of the cavity. The heater could be a thermofoil heater and the temperature sensor a platinum resistance thermometer, for example.

Limitations of using blackbodies are the mass, power, and size requirements. Blackbodies can be used from the UV to the IR, but the radiation is typically less stable at UV due to the high temperatures needed to operate at short wavelengths and the need to adjust the opening to the cavity [6]. Blackbody sources typically take about an hour to stabilize to the desired temperature in order to accurately operate at the desired output [9]. In order to have a blackbody ready to be viewed by the instrument for calibration, it requires a stable operating temperature prior to and during the calibration tasks. The device can be inconveniently large especially when using the cavity type of blackbody. For space applications it is desirable to keep size, mass, and power to a minimum.

2.2 Light Emitting Diodes

Light emitting diodes (LEDs) are semiconductors that convert a forward electric current into light. LEDs are made of p and n regions in various semiconductor materials with carriers being injected across the junction and diffusing into the p and n regions. When the minority carriers recombine with the majority carriers, this recombination gives rise to the light emission. LEDs are designed by fabricating the pn junction with a semiconductor of the type known as a direct-band gap material [10]. LEDs that are commercially available operate in the 210 nm to 1 µm range. One of the limiting factors of using LEDs as calibration sources is the availability of devices at mid-IR (MIR) to the far-IR (FIR) wavelengths.

2.3 Lasers

A laser is a device that emits light through a process of optical amplification based on the stimulated emission of photons. One general classification that describes a laser is the type of the gain medium. The gain medium is one in which population inversion is created. A population inversion is the state where there are more molecules or atoms in an excited state than in a lower energy state. A population inversion is achieved by pumping the gain medium, which can occur by optical absorption, electrical current, or by another

means of exciting the molecules or atoms [11]. Lasers require a population inversion to obtain amplified optical emission. The gain media can be of various states: solid, liquid, or gas [12]. The physical construction, electrical power feed, and the output power, as well as the ability to operate in continuous or pulsed mode, are distinct for each type of laser [13].

The population of excited atoms in gas lasers can be obtained by having an electric current discharged through the gas. They can produce high output power, depending on the gas to be pumped. Another type of laser is a chemical laser. These lasers obtain population inversion using the energy of a chemical reaction. Chemical lasers are mainly used for cutting and drilling purposes as they can have an output power density in the megawatts.

Semiconductor lasers are based on the gain media being the semiconductor, where the optical gain is usually achieved by stimulated emission at an interband transition under conditions of a higher carrier density in the conduction band. The gain medium is a semiconductor crystal or glass that can be doped, customized by introducing impurities, to the requirements of the desired laser characteristics.

Lasers can either be operated in a pulsed mode or a continuous-wave (CW) mode. The pulsed mode operates by pumping the gain medium in pulses. This may occur by turning the driving current to the laser device on and then off in a semiconductor laser, for example. They can also emit pulses by altering the quality or "Q" of the resonance cavity. In a CW laser the pumping occurs continuously, as in a current set to a particular value, for example. Some lasers are designed to operate in pulsed mode and some in continuous-wave mode only, but many can operate with both driving techniques.

A majority of solid-state and gas lasers rely on narrow optical transitions connecting discrete excitation energy levels. Semiconductor diode lasers rely on transitions between energy bands in which conduction electrons and valence band holes recombine across the band gap as seen in Figure 2.1. The band gap determines the emission wavelength of the device [14].

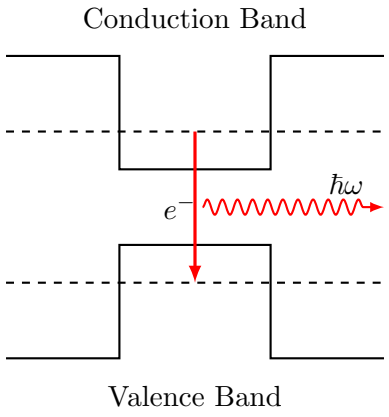

Fig. 2.1: Interband optical transition.

A unique type of the semiconductor laser is the QCL. A QCL makes use of discrete electronic states arising from the quantum confinement, normal to the layers, in nanometer-thick semiconductor heterostructures grown by molecular beam epitaxy [14]. Quantum cascade lasers use a periodic series of thin layers of varying material composition to form a superlattice as shown in Figure 2.2. This superlattice introduces a varying electric potential across the length of the device, which implies that there is a probability of electrons occupying different positions over the length of the device material. This technology facilitates the wavelength to be determined by the quantum confinement, which can be tailored, over a wide spectral range from the MIR to the submillimeter wavelength region, "a portion of the spectrum not easily accessible with diode lasers" [14].

QCL devices come in three main forms: Fabry-Perot (FP) QCLs, Distributed-feedback (DFB) QCLs, and external cavity (EC) QCLs. These QCL devices have different characteristics in how the gain media is used to determine the spectral output characteristics.

Fabry-Perot QCL devices are made by cleaving the ends of the superlattice gain material forming mirrors for a Fabry-Perot resonator cavity. Because of the design of FP-QCLs, they support multi-mode operation.

Distributed-feedback QCL devices are made in the same manner as FP-QCLs, except that there is a reflecter built into the waveguide to isolate a single emission mode. An

interesting characteristic of DFB-QCLs is that they may be tuned by changing the current through the device to within 1% of the center wavelength [15].

The last type of QCL device is the EC-QCL. The EC-QCL device is made by cleaving the ends of the crystal and then applying an anti-reflective (AR) coating on the ends. The AR provides the ability to place the supperlattice gain medium inside an external resonator. With the use of an external resonator the QCL may be tunable to greater than 35% of the center wavelength [15, 16].

With the superlattice design and wide optical gain spectrum, the QCL output can be tailored to fit needs of many applications. In the case of using a QCL as a calibration source, a desired output may be a narrow or wide bandwidth, depending on the application. A FP-QCL, referred to as a multimode laser, has a broad band emission similar to the one in Figure 2.3(a). A DFB-QCL design is a single mode laser. The output emission of a DFB-QCL has a narrow spectral bandwidth as shown in Figure 2.3(b) [17]. Either type of QCL can operate in the pulsed or continuous-wave mode. The EC-QCL spectral output is determined by its external resonator.

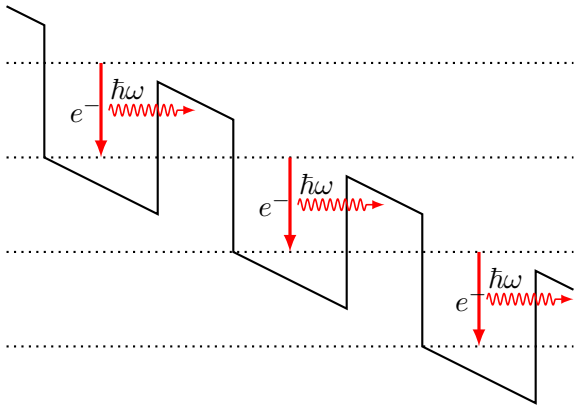

Fig. 2.2: Cascade transitions.

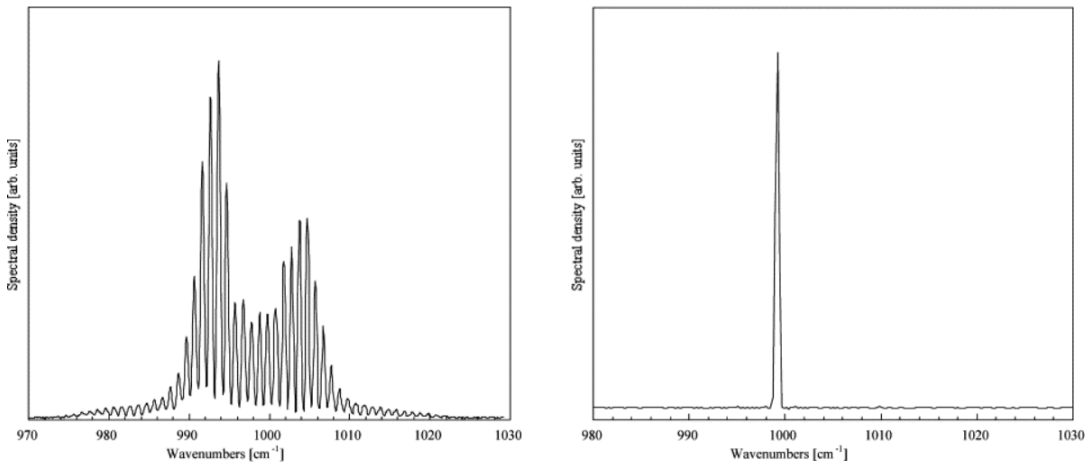

(a) Fabry-Perot (b) Distributed-feedback

Fig. 2.3: Different quantum cascade laser spectral characteristics.

Chapter 3

Quantum Cascade Laser Control Electronics

QCLs require stable drive current and a constant temperature in order to maintain stable power output. If the inputs to the QCL are not stable, the output characteristics of the laser will not be stable or reproducible. If the drive current to the QCL changes during operation, it can induce what is referred to as "beam steering." Beam steering is usually accompanied with a significant change in the spectral characteristics [18]. Any change in change in drive current will affect the emitted power.

Temperature stability is also an issue for the QCL devices. Unlike early QCLs, which operated at cryogenic temperatures, many QCLs on the market today are designed to operate optimally at room temperature, which is approximately 300 K. If the driver provides a stable output but the temperature changes, then the laser output will not be stable or reliable. The two critical factors to consider in designing a QCL controller are the current and temperature control.

3.1 PNNL QCL Current Controllers

Quantum cascade laser drive electronics are designed using transistor based technology, for filtering and noise reduction, with current control circuitry [19–21]. The controllers also achieve a low noise level using LC filter designs and other noise eliminating factors [22]. The PNNL current control performance noise levels achieved under CW operation is 1-2 ppm/°C and under pulsed operation 15 ppm/°C [22].

3.2 Laboratory QCL Temperature Controllers

Temperature control for most QCLs is based on a thermoelectric cooler (TEC) design combined with a heat transfer system. The TEC is used to keep the temperature at an

accurate set-point while the heat transfer system is used to conduct heat to an exterior heat sink. For use as calibration sources, QCLs should use a cooling system to keep the temperature at a constant set-point.

A typical TEC control circuit is based on a set-point temperature (voltage reference) and uses an H-bridge or power amplifiers to drive the current direction in forward or reverse. When the TEC temperature goes above the set-point temperature, then the H-bridge or power amplifiers will decrease the temperature by reducing or reversing the current direction to the TEC [23].

Chapter 4

Quantum Cascade Laser and Test Station

To help understand QCLs and how to operate them a Fabry-Perot QCL from Thorlabs was acquired. This QCL has maximum operating current of 1100 mA and power output of 500 mW.

4.1 Quantum Cascade Laser Specifications

The 4.55 µm QCL has a spectral response shown in Figure 4.1. This figure shows a center wavelength at 4.61 µm with a bandwidth $\Delta\lambda \simeq 0.1$ µm. The output power of the QCL changes according to the amount of current through the device as shown in the light-current-voltage (LIV) curve in Figure 4.2.

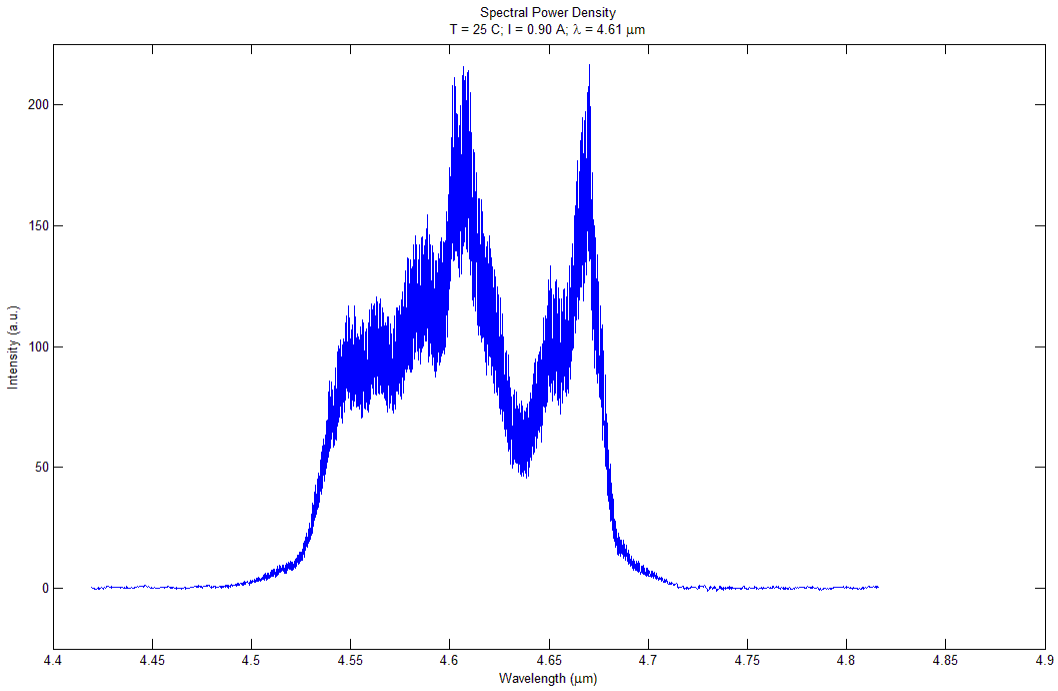

Fig. 4.1: M1013H spectral power density at CW (courtesy of Thorlabs).

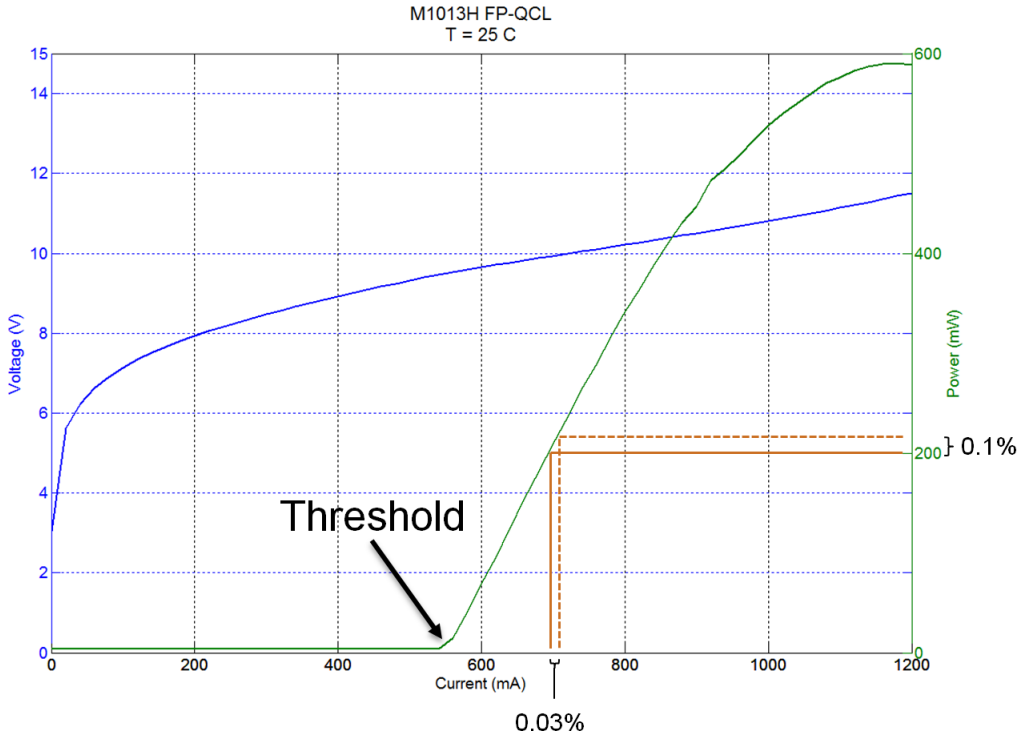

Fig. 4.2: M1013H LIV curve at CW (courtesy of Thorlabs).

The LIV curve shows the characteristics of the QCL. The threshold current can be determined from the LIV curve. The threshold current is the current at which the QCL begins to lase and is characterized by the power output of the QCL increasing at around 550 mA. After finding the threshold current, it is useful to find the slope efficiency of the QCL. The slope efficiency is the slope of the power output to current input after the threshold. Calculating the slope using current levels of 550 and 900 mA with associated power outputs of 0 and 560 mW results in a slope efficiency of 1.02 W/A.

4.2 Test Station Setup

To gain experience with the QCL a test station was configured see Appendix A. The test station configuration consists of a current controller, TEC controller, a water circulator, computer, QCL mount, laser power meter, and a data acquisition unit (DAQ). A flow chart of the test setup is seen in Figure 4.3. The test station facilitates the capability to measure the QCL's power output.

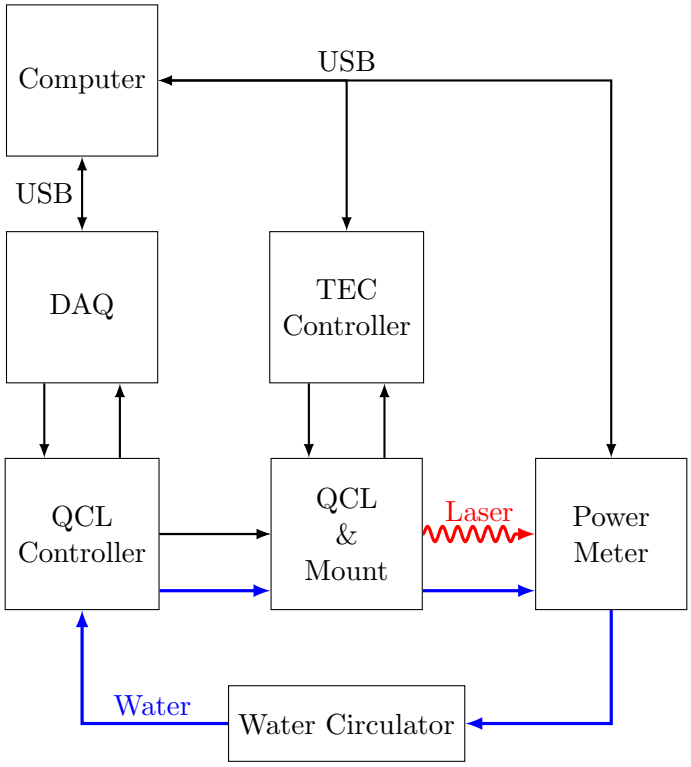

Fig. 4.3: Test station flow chart.

In this test station National Instrument's LabVIEW® was used to create the software for controlling the current levels to the QCL, and to log data points from the connected devices see Appendix B for a view of the user interface. A test control sequence in the LabVIEW® program takes a set of desired current levels. For example a test sequence can consist of [0, 0, 350, 450, 550, 575, 600, 625, 650, 0, 0, 0, 0] where each number is representative of milliamps through the QCL. The program then takes this control sequence and steps through it at a user specified interval. If the time is set to fifteen seconds then the program steps through the control sequence at fifteen second intervals, for example. The user specified interval should be long enough to allow for the temperature of the QCL to stabilize to the temperature set point. A test sequence is repeated a number of times. The recorded data points are then analyzed using MATLAB®. A script in MATLAB® takes the last five seconds of each step to calculate average and standard deviations in the QCL power output. These data facilitate the interpretation of power output stability and

repeatability.

The LabVIEW® program can control the current in either CW or pulsed operation. Studies at PNNL show that power output stability is better with pulsed operation [24]. Stability tests were also performed at USU in the pulsed operation mode. The resulting power output stability at various frequencies are shown in Figures 4.4 and 4.5. These figures show that the QCL power output is stabilized when running at modulated rather than CW mode. These tests were repeated multiple times with the same result in each case.

QCL devices need to be stable to be considered as calibration sources. The published results from PNNL and tests performed at USU both show that running QCLs in a pulsed manner can produce a more stable power output than operation in CW mode. Therefore, for QCLs to be used as calibration sources, it is generally best to operate them in pulsed operation.

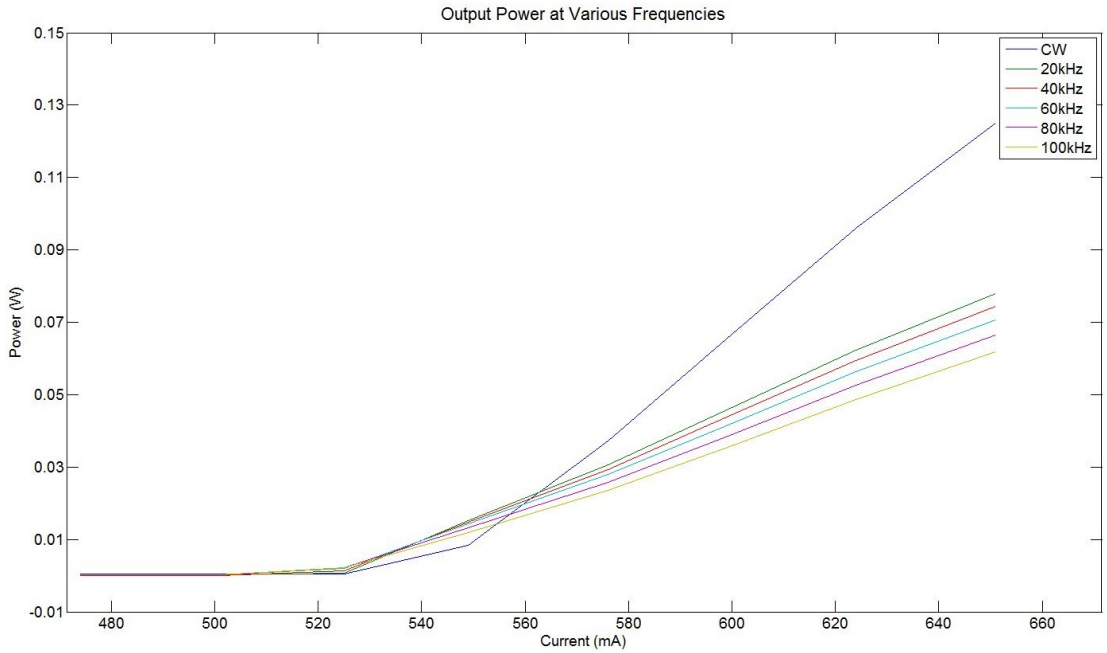

Fig. 4.4: Multiple frequency test average power.

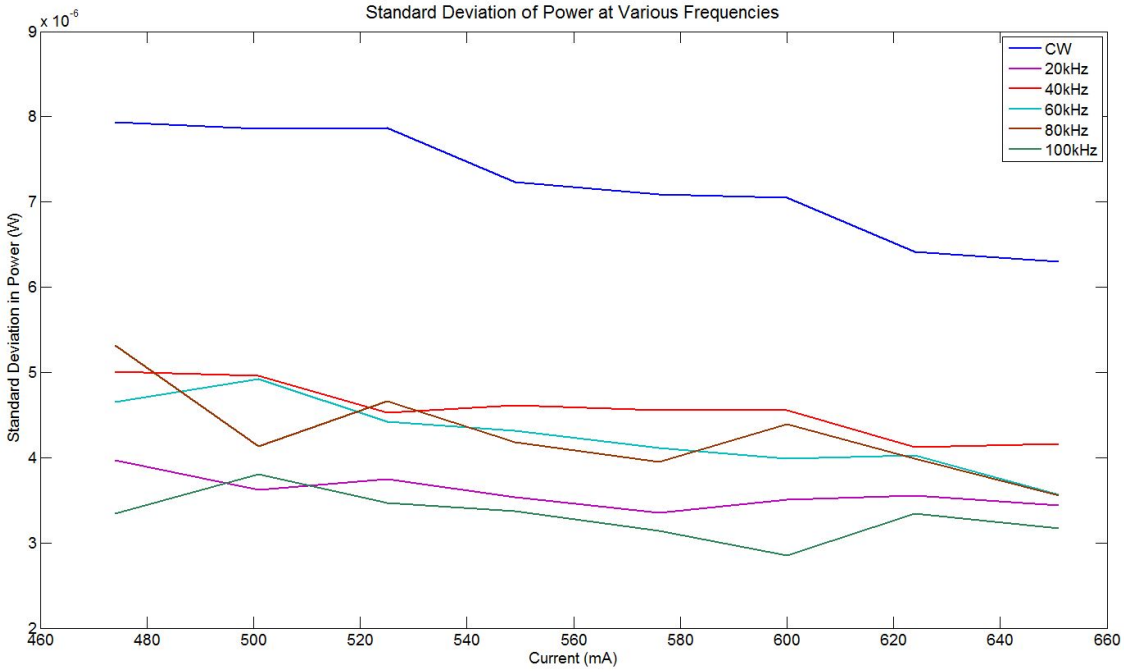

Fig. 4.5: Multiple frequency test standard deviation of power.

Chapter 5

Flight Electronics Design

5.1 Background of Flight Design QCL Driver

The precision QCL controller design uses PNNL's design as a starting point. A comprehensive study was performed to ratify radiation hardened or space qualified electronic parts for the design.

5.2 Flight Circuit Overview

A simplified schematic of the precision current controller for the QCL is shown in Figure 5.1. Precautions were taken to ensure minimal drifts in voltages throughout the system. This ensures long term stability of the overall system. Active filters are used throughout the system to eliminate noise transients from the voltages sources to the sensitive components. The goal is to achieve a QCL power output stability of 0.1% over a wide range of environmental conditions.

5.2.1 Theory of Operation

Using a universal asynchronous receiver/transmitter (UART) protocol, commands are sent to the field-programmable gate array (FPGA). The FPGA controls the address lines to the mux/demux, based upon the received commands see Appendix C for FPGA simulations. The address lines to the mux/demux are used to determine which voltage line will be used from the precision resistor network voltage buffer. Using the voltage from the resistor network voltage buffer the mux/demux then feeds this desired voltage level to the current controlling amplifier the OP37S op-amp. The OP37S op-amp then takes the voltage from the mux/demux and uses the voltage feedback from the 4-wire resistor to determine the voltage at the gate of the MOSFET. The voltage applied to the gate of the MOSFET will

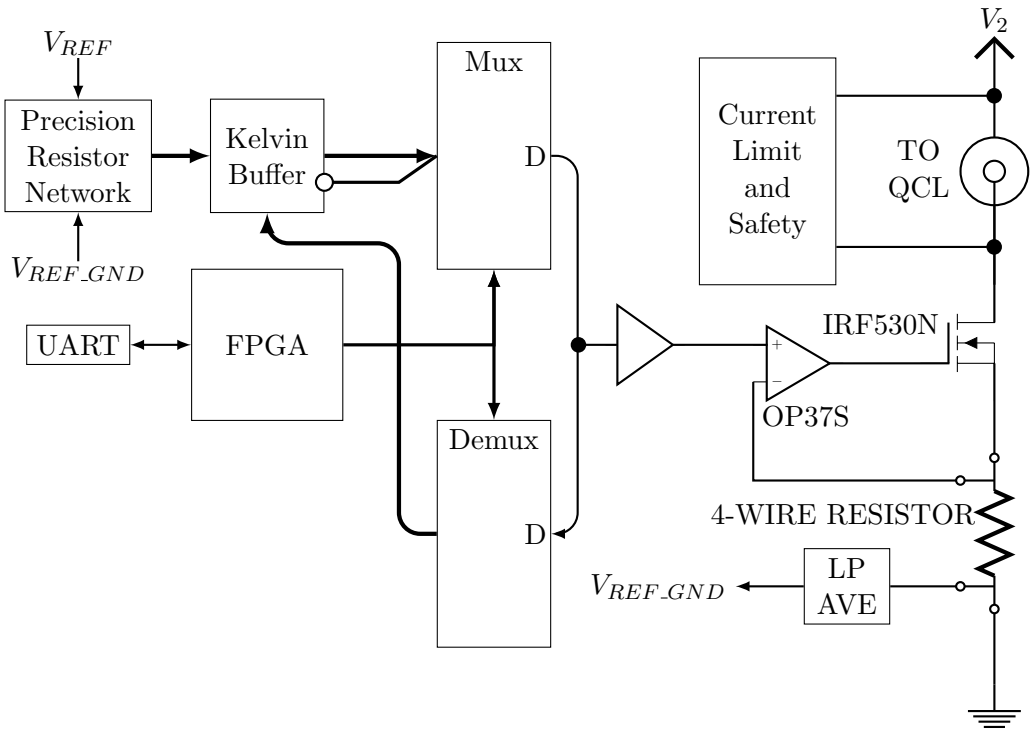

Fig. 5.1: Circuit overview.

determine the current through the MOSFET, which will be the same current through the QCL and the 4-wire resistor. The mux/demux turns the QCL off when a ground voltage is selected as the reference voltage. The selections of voltages above ground are associated with a specific current level through the QCL. A pulsed mode is achieved by switching between a channel having a voltage level greater than zero and ground. Controlling the mux/demux enables the controller to facilitate operation in CW or pulsed modes with the same circuitry.

5.2.2 Current Controller

The purpose of this circuit is to precisely control the current through the QCL. The circuitry that controls this current is shown in Figure 5.2. The positive side of the OP37S is fed a selected voltage reference. This voltage reference is compared to the voltage from the top of the 4-wire resistor. If the voltage reference does not match the voltage at the top of

the 4-wire resistor, then OP37S op-amp changes the gate voltage applied to the MOSFET until there is a voltage match. For this current to be precise, the following sections will describe ways to maintain precision in the system as to the current control for the QCL.

5.2.3 Mux/Demux Configuration

In Figure 5.1, it can be seen that the voltage from the mux/demux configuration is the control signal for the current controller. The mux/demux configuration was designed to compensate for any losses due to the on resistance of the mux. The diagram in Figure 5.3 will be used to derive equations and show how this compensation works.

In ideal op-amp theory, the voltage at the positive (V_p) and negative (V_n) terminals is equivalent, which is expressed in Equation (5.1). The current into the positive (I_P) and negative (I_n) terminals is zero as expressed in Equation (5.2).

$$V_p = V_n \tag{5.1}$$

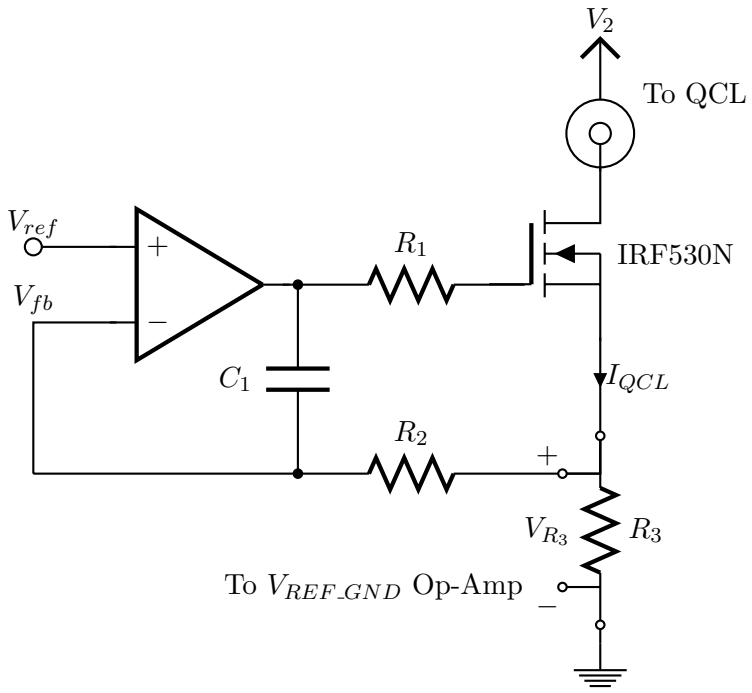

Fig. 5.2: Basics of current control.

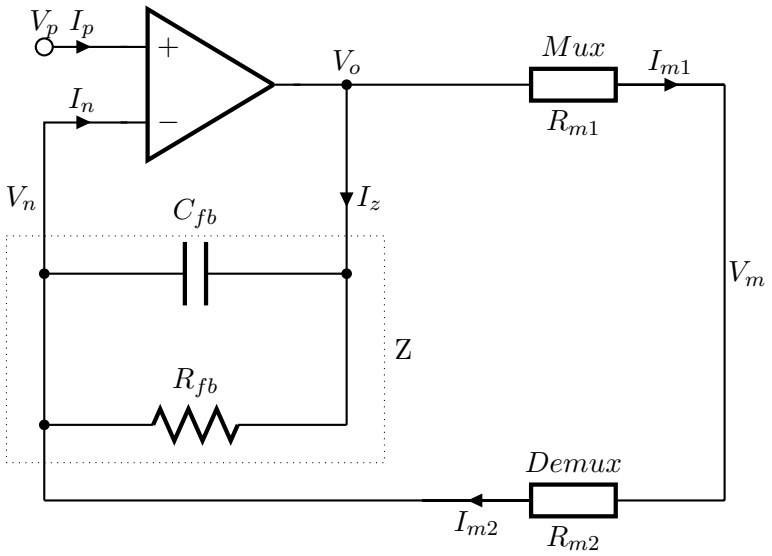

Fig. 5.3: Mux/demux diagram.

$$I_p = I_n = 0 \tag{5.2}$$

Now finding the current through the mux (I_{m1}) and demux (I_{m2}) according to the ON resistance is shown in Equations (5.3) and (5.4).

$$I_{m1} = \frac{V_o - V_m}{R_{m1}} \tag{5.3}$$

$$I_{m2} = \frac{V_m - V_n}{R_{m2}} \tag{5.4}$$

The capacitor and resistor are combined into one equivalent impedance as shown in Equation (5.5) where S is the Laplace variable. Finding the current I_z is shown in Equation (5.6).

$$Z = \frac{R_f}{S \cdot C_f \cdot R_f + 1} \tag{5.5}$$

$$I_z = \frac{V_n - V_o}{Z} \tag{5.6}$$

Summing the currents into the negative terminal of the op-amp results in Equation (5.7). Inserting Equations (5.2), (5.4), and (5.5) into (5.7) will produce Equation (5.9).

$$I_n = I_z + I_{m2} \tag{5.7}$$

$$0 = I_z + I_{m2} \tag{5.8}$$

$$0 = \frac{V_n - V_o}{z} + \frac{V_n - V_m}{R_{m2}} \tag{5.9}$$

The current in the mux and demux must be equal because they are connected in series as shown in Equation (5.10). Using Equations (5.3) and (5.4) in Equation (5.10) results in Equation (5.11). Solving Equation (5.11) for V_o results in Equation (5.12).

$$I_{m1} = I_{m2} \tag{5.10}$$

$$\frac{V_o - V_m}{R_{m1}} = \frac{V_m - V_n}{R_{m2}} \tag{5.11}$$

$$V_o = \frac{R_{m1}(V_m - V_n)}{R_{m2}} + V_m \tag{5.12}$$

Using Equations (5.9) and (5.12) results in Equation (5.13) and solving for Vm results in (5.14). The relationship between the voltage out of the mux to that of V_p is reduced to (5.15). From this calculation, it can be said that the voltage going into the mux configuration is the same as that of the voltage coming out. A unity gain buffer is then used to buffer the voltage output of the mux/demux configuration, which feeds the voltage to the OP37S as the reference voltage for the current set point.

$$0 = \frac{Vn - \frac{R_{m1}(V_m - V_n)}{R_{m2}} - V_m}{z} + \frac{V_n - V_m}{R_{m2}} \tag{5.13}$$

$$0 = (V_p - V_m)\frac{z + R_{m1} + R_{m2}}{R_{m2}z} \tag{5.14}$$

$$V_p = V_m \tag{5.15}$$

5.2.4 Four-Wire Resistor

The use of a 2-wire resistor for current sensing would result in greater error in the system. This error would come into play because copper can have a TCR of 3930 ppm/°C [25]. If the traces and leads were managed to have a resistance of around $10\,\text{m}\Omega$ then the change in resistance would be associated to a 0.39%/°C [25]. Using a $1\,\Omega$ current sense resistor in association to the copper TCR will produce errors of 39 ppm/°C, which compromises the desired stability of the current controller. To greatly reduce this error a 4-wire resistor was chosen. This 4-wire resistor provides for the capability to compensate for possible errors from the copper traces. A technique used by Taubman was used to measure the ground side of the 4-wire resistor using the Kelvin connections [24].

5.2.5 V_{REF_GND} Network

The V_{REF_GND} is a Kelvin net, which is a network that draws minimal current, ensuring minimal voltage drop and temperature-induced variations [24]. The V_{REF_GND} is used to account for discrepancies due to the copper traces or wires after the 4-wire resistor to ground. This proves useful as the bottom side of the 4-wire resistor is close to ground facilitating V_{REF_GND} to act as the ground for sensitive circuits used to maintain stability and precision. V_{REF_GND} is referenced to the ground side of the precision resistor network and precision voltage reference using Kelvin buffers as shown in Figure 5.4. Kelvin buffers are used to sample sensitive signals and compensate voltage drops in traces. For the Kelvin buffer, the feedback resistor is generally larger than the output resistor. Kelvin buffers use

traces that go to the same node shown as *Destination Node* in Figure 5.4. This ensures proper feedback for compensation due to voltage drops in traces. The op-amps used for the Kelvin buffers have high input impedance, generally greater than 10 MΩ, a low input bias current, and low and stable voltage offset.

When the laser is operated in CW or pulsed modes V_{REF_GND} is generated by passing the low side of the 4-wire resistor through an active low-pass filter. The use of V_{REF_GND} as the ground reference for the precision voltage reference and precision resistor network helps eliminate any errors in current measurement due to losses in the traces following the 4-wire resistor. This generation of V_{REF_GND} is easily shown for a CW mode because of a unity gain in the filtering device, but when the operation mode is changed to pulsed, the gain of the filtering device needs to change. The pulsed mode used in this case is for 50% duty cycle square waves.

The pulsed mode generation of V_{REF_GND} takes the average of the waveform. The average of the waveform is found by passing the signal through a low-pass filter targeted with a corner frequency of 150 kHz and a third-order Bessel low-pass voltage-controlled voltage-source filter at a corner frequency of 1.5 kHz [26]. The latter filter frequency is to filter out the modulation frequency of 40 kHz or other frequencies greater than 1.5 kHz. With the configuration for pulsed mode the active filter has a gain of two, which accounts for the averaging of the pulsed signal. This design accounts for loss in the ground trace from the 4-wire resistor. It provides precision voltage levels for the desired current through the QCL and provides a stable QCL output.

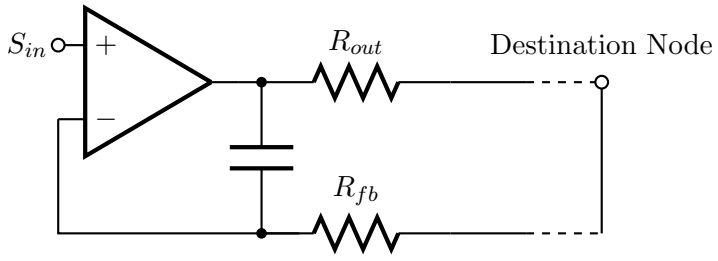

Fig. 5.4: Kelvin buffer example.

5.2.6 Electronics Study

Electronics used in flight designs should be qualified to be operational in the space environment. This environment has many factors that can affect electronic functionality. These factors include, but are not limited to, extreme temperature changes, vacuum, radiation, and electromagnetic fields.

Electrical components that have been used on previous flight configurations with resulting good performance are prime choices. Many components chosen for the design of this current controller were used in past flight missions such as WISE, SABER, and others. Some components used in the design follow the same fabrication process as space qualified parts but do not carry certifications. The latter components were studied and selected for budgeting reasons.

5.2.7 Key Components

Key components used in the reference design were an ultra-precision voltage reference, an 18-bit low-noise digital-to-analog converter (DAC), a 1 pC charge injection 4-channel multiplexer, an ultralow distortion ultralow noise op-amp, a power MOSFET with a total gate charge of 11 nC, and an ultra-high precision Z-Foil power resistor with low temperature coefficient of resistance (TCR).

Precision Voltage Reference

The ultra-precision voltage reference from Linear Technology, the LTZ1000A, was used in the reference design. This device is very stable with a 2 $\mu V/\sqrt{kHr}$ long term stability and a drift of 0.05 ppm/°C [27]. Although this device is not tested for the space environment some research shows that it outperforms space qualified voltage references. According to B. G. Rax et al. the LTZ1000A showed "that it is possible to obtain far better performance in a radiation environment with alternative design approaches" [28]. Due to the performance of this device it was decided to use the same precision voltage reference.

Creating the Precision Voltage Levels

The reference design used an 18-bit (DAC). This 18-bit low-noise DAC provides for a dynamic range of voltages to be used for current control, but it is not designed for the space environment. This device also supports using a voltage reference and reference ground, which is a useful feature that allows for compensation due to ground reference changes.

Space qualified DACs are either limited in available bits or their cost exceeded the project budget. After considering this issue, it was decided to create a custom resistor network to produce the desired voltage outputs.

Creating a custom network is simple in theory, but resistors can be noisy and can change resistance with a change in current, temperature, voltage, or a combination thereof. With these changes in mind it was decided to discuss the matter with some experts at Vishay Precision Group. The discussion with Vishay led to a decision to use one of their custom packages, where a custom resistor network may be designed with a given criteria. This custom resistor network is made up of Ultra high precision Bulk Metal® Z-Foil chip resistors with a TCR of 0.05 ppm/°C. Having a custom resistor network in the same package has the advantage of temperature tracking between the resistive elements, rendering the effects of TCR insignificant.

Selecting the Precision Voltage Levels

The decision to use a resistor network to produce the precision voltage levels created need for a multiple input multiplexer. After some consideration it was decided the 16 inputs would be sufficient. This allows for 15 different voltage levels plus ground. The search for a multiplexer resulted in the HS1840ARH, which can operate at the desired modulated frequencies or CW modes. The propagation delay of the output of the HS1840ARH is approximately 0.6 µs, about 3 to 4 times larger than the multiplexer used in the reference design.

The HS1840ARH was tested under various temperature conditions to verify that the rise and fall times of the device would preserve the integrity of a square wave at 40 kHz. The results of the tests are shown in Table 5.1 and Figures 5.5 and 5.6, which validates

that there is about a 1 ppm/°C delay on the rising edge and falling edge compared to the input signal.

Low-Distortion Op-Amp

The op-amp used in the design was required to have a around a 12.5 V/µs slew rate, and a 120 dB common-mode rejection ratio (CMRR). These factors led to the selection of the OP37S, which has a minimum slew rate 11 V/µs and CMRR of 114 dB.

Table 5.1: HS1840ARH temperature results.

Temp	Prop Delay 1		Prop Delay 2		Pos Width		Sample Size
	MEAN	STD	MEAN	STD	MEAN	STD	
−20 °C	0.2134 µs	2.4260 ns	0.3134 µs	1.6260 ns	12.643 µs	3.5050 ns	5.213k
25 °C	0.2531 µs	1.6080 ns	0.3556 µs	3.3490 ns	12.643 µs	3.9950 ns	2.165k
60 °C	0.2938 µs	1.9480 ns	0.4030 µs	3.7910 ns	12.651 µs	5.3000 ns	7.932k
80 °C	0.3037 µs	2.8330 ns	0.4095 µs	3.4400 ns	12.650 µs	5.5470 ns	5.208k

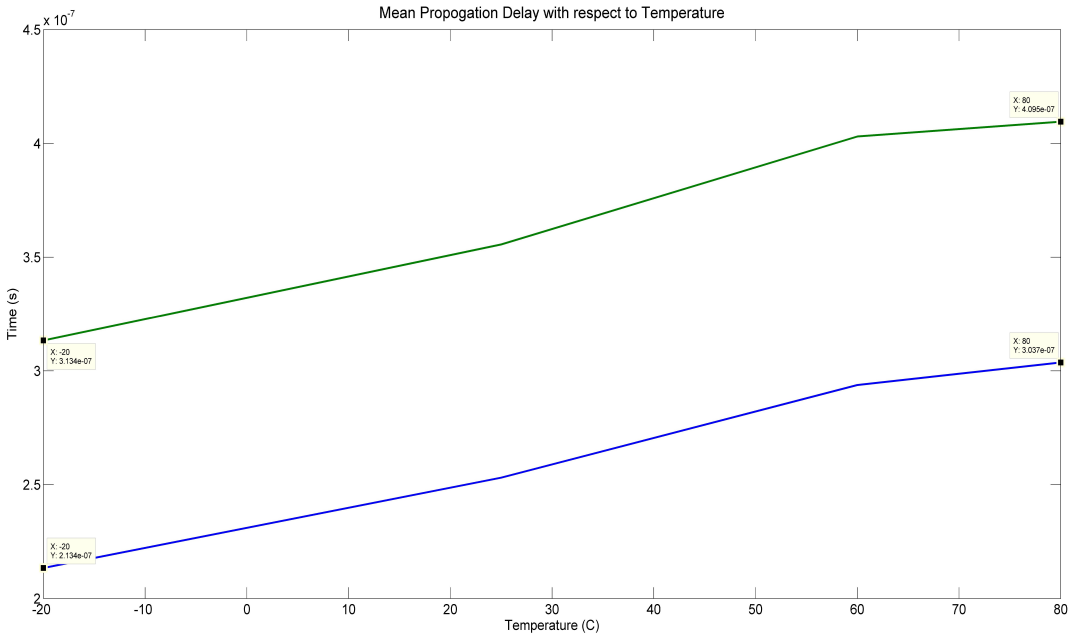

Fig. 5.5: Mean of first and second propagation delays.

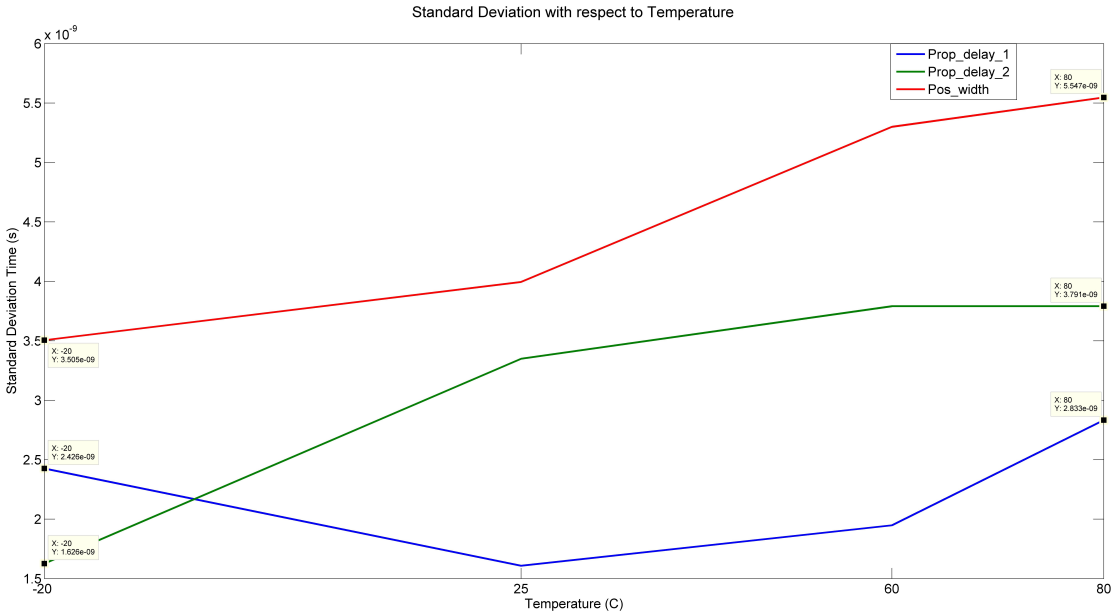

Fig. 5.6: Standard deviation of first and second propagation delays.

Due to the cost of the OP37S, it was decided to use the device in the same family with the part number OP37GPZ, which turns out to be identical in performance to the OP37S except for the price of the product. In this instance a space qualified part was chosen and then a commercial part was used with an identical specification.

Current Controlling

The selection of a metal-oxide-semiconductor field-effect transistor (MOSFET) having a high current rating and a low input capacitance that is space qualified is limited. The IRHNJ67234 was selected which has gate charge of 37 nC compared to the 11 nC of the commercial part used in the reference design. Again, this part was used as a basis for finding a commercial part to use in the prototyping of the current controller.

The final decision to use the IRF530NPBF, which has a total gate charge capacitance of 37 nC, will show that a MOSFET with this gate charge can be controlled efficiently using a modulated signal greater than the 1.5 kHz.

Current Sense Resistor

The QCL calibration source may draw up to an amp of current. This could result in large power dissipation in the sense resistor. It is desirable to limit power consumption in a circuit intended for space application. Therefore, a 1 Ω sense resistor was chosen to reduce the power dissipation in the board. The package chosen for the space application is a hermitically sealed 1 Ω resistor in a 4-pin package, the hermitic sealing helps preserve performance even in vacuum environments where out gassing may be an issue.

Other Components

All other components in the design could use space qualified parts. Some components such as passive components are all commercial or military level devices. The main concern is active parts, since they will change characteristics due to the space environment.

Chapter 6

Flight Electronic Simulations and Uncertainty Analysis

After the design of the QCL controller, simulations using LTspice were performed to analyze the output noise of the electronics. Simulations were useful in determining the finalized controller design.

6.1 Quantum Cascade Laser Controller Simulations

Simulations were performed on the current controller to prove the control concept, and analyze noise characteristics with pulsed and CW operation. The results of the current control simulations showed the ability to limit the noise to below 25 µV or 25 µA.

6.2 Noise Output of Active Filters

Active filters based on capacitance multipliers were designed using PNNL's design as a starting point. The active filters are used to reduce the noise at the frequency of operation, and isolate noise from going back into the voltage supplies. The noise performance at frequencies approaching 1 kHz are about 350 nV. At frequencies greater than 1 kHz, the noise drops very quickly. At frequencies greater than 6 kHz the noise is about 2 nV. See Appendix D for simulations and results. With the pulsed mode running at 40 kHz the noise of the voltage inputs to the operational amplifiers is approximately 2 nV. This ensures that the noise on the power rails of the device is not a significant factor for the amplifiers.

6.3 Monte Carlo Temperature Noise Analysis

A Monte Carlo temperature noise analysis was simulated on the current design. This noise analysis takes into account the critical parts of the circuitry with special attention on the precision resistor network and the current sense resistor. The resulting noise analysis

showed a variation of ± 200 ppm/°C in error output from the measured error of 12 µV at 40 kHz.

6.4 Uncertainty Analysis of Laser Power Output

In analyzing the current through the QCL it can be assumed that the power output is averaged as the current is being modulated. The variable of interest is P_{meas}, which is the measured output power of the QCL. Using the slope efficiency (K_1) and threshold current (K_0) as defined in Section 4.1 with the sensitive components (H_{char}) and sense resistor (R_{sense}) a transfer function can be formed. The flow for the formation of the tranfer function can be seen in Figure 6.1.

The derivation of the transfer function with focus on sensitive components results in Equation (6.1). H_{char} is defined by Equation (6.2) with terms defined as follow:

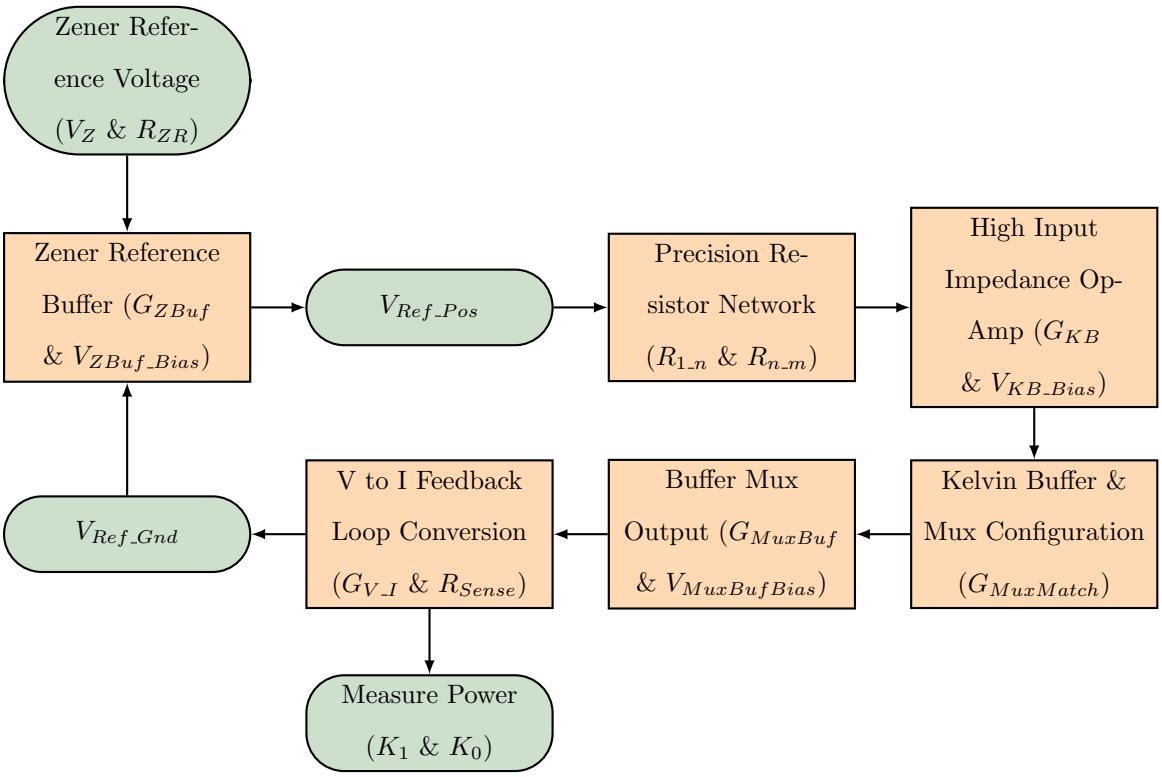

Fig. 6.1: Transfer function flow chart.

- $G_{V\_I} \triangleq$ gain of the voltage setpoint to the current through the MOSFET,
- $G_{MuxBuf} \triangleq$ gain of op-amp buffer after mux,
- $V_{MuxBufBias} \triangleq$ op-amp buffer bias voltage,
- $G_{MuxMatch} \triangleq$ difference in mux/demux on resistance,
- $G_{KB} \triangleq$ gain of kelvin buffer op-amps,
- $V_{KB\_Bias} \triangleq$ kelvin buffer op-amp bias voltage,
- $REF \triangleq$ operating voltage level for current control,
- $R_{1\_n} \triangleq$ precision resistor values 1 through n,
- $R_{n\_m} \triangleq$ precision resistor values n through m,
- $G_{ZBuf} \triangleq$ gain of zener voltage buffer op-amp,
- $V_{ZBufBias} \triangleq$ buffer op-amp bias voltage,
- $V_Z \triangleq$ zener voltage,
- $R_{ZR} \triangleq$ precision resistor after zener,
- $I_Z \triangleq$ current through zener,

$$P_{meas} = K_1 \left(\frac{H_{char}}{R_{Sense}} \right) - K_0 \tag{6.1}$$

$$H_{char} = G_{V\_I} \left[G_{MuxBuf} \left[G_{MuxMatch} \left[G_{KB} \left[REF \right] + V_{KB\_Bias} \right] + V_{MuxBufBias} \right] \right] \tag{6.2}$$

$$REF = \left(\frac{R_{1\_n}}{R_{1\_n} + R_{n\_m}} \right) \left[G_{ZBuf} (V_Z + R_{ZR} I_Z + V_{Ref\_Gnd}) + V_{ZBufBias} - V_{Ref\_Gnd} \right] \tag{6.3}$$

From this transfer function a sensitivity vector S is defined as the deviation of each parameter due to temperature. Taking partial derivatives of the transfer functions facilitates the formation of a covariance matrix. With the covariance matrix and sensitivity vector the overall uncertainty is expressed in Equation (6.4).

$$(dP_{meas})^2 = S \cdot CV \cdot S^T \tag{6.4}$$

The numerical evaluation of Equation (6.4) results in a power uncertainty of 20 µW/°C at a power output of 233 mW. For a power output of 410 mW the uncertainty becomes 25 µW/°C. When the QCL is operated at the maximum power output of 500 mW, the uncertainty is approximately 27 µW/°C, which calculates to a stability of 0.005%/°C. This analysis shows that the QCL output can be kept well within a 0.01%/°C of power output stability. The calculated stability facilitates a temperature change of ± 10 °C and still be within the 0.1% power output stability goal.

Chapter 7

Conclusion

This research shows that QCLs can be used as calibration sources in space flight applications. In order to use a QCL as a calibration source, it requires a precision current controller that has minimal errors due to temperature variations. The controller should operate in both CW and pulsed modes to allow for further studies into the best driving technique for the QCL to be used as a calibration source. With a very stable voltage and current control the reproducibility and stability of QCLs is improved greatly allowing them to be used as a calibration source. The uncertainty analysis shows the ability to control the QCL's power output to well within the desired 0.1 % with a $\pm$ 10 °C change in the current controller electronics.

References

[1] A. Yamashita, T. Dotani, M. Bautz, G. Crew, H. Ezuka, K. Gendreau, T. Kotani, K. M. adn C Otani, A. Rasmussen, G. Rickar, and H. Tsunemi, "Radiation damage to charge coupled devices in the space environment," *IEEE Transactions on Nuclear Science*, vol. 44, no. 3, pp. 847–853, June 1997.

[2] C. L. Wyatt, *Radiometric Calibration: Theory and Methods*. New York: Academic Press, Inc., 1987.

[3] J. J. Tansock, S. Hansen, K. Paskett, A. Shumway, J. Peterson, J. Stauder, L. L. Gordley, Y. Wang, M. Melbert, J. M. R. III, and M. G. Mlynczak, "Saber ground calibration," *International Journal of Remote Sensing*, vol. 24, no. 2, pp. 403–420, 2003.

[4] T. L. Myers, B. T. Brooks, B. D. Cannon, and N. Ho, "Fy07 final report for calibration systems," Pacific Northwest National Laboratory, Richland, WA (USA), Technical Report PNNL-17254, Dec. 2007, dOE Contract Number: AC0576RL01830. [Online]. Available: www.osti.gov/scitech/biblio/1035012

[5] Wikipedia, "Black body," Wikipedia, The Free Encyclopedia, Wikipedia, The Free Encyclopedia, Mar. 2013. [Online]. Available: http://en.wikipedia.org/w/index.php?title=Special:Cite&page=Black_body&id=544455296

[6] V. I. Sapritsky, B. B. Khlevnoy, V. B. Khromchenko, B. E. Lisiansky, S. N. Mekhontsev, U. A. Melenevsky, S. P. Morozova, A. V. Prokhorov, L. N. Samoilov, V. I. Shapoval, K. A. Sudarev, and M. F. Zelener, "Precision blackbody sources for radiometric standards," *Applied Optics*, vol. 36, no. 22, pp. 5403–5408, 1997.

[7] W. E. Forsythe and E. Q. Adams, "Radiating characterisitcs of tungsten and tungsten lamps," *Journal of the Optical Society of America*, vol. 35, no. 2, pp. 108–113, 1945.

[8] F. A. Best, H. E. Revercomb, R. O. Knuteson, D. C. Tobin, S. D. Ellington, M. W. Werner, D. P. Adler, R. K. Garcia, J. K. Tayler, N. N. Ciganovich, W. L. Smith, G. Bingham, J. D. Elwell, and D. K. Scott, "The geosynchronous imaging fourier transform spectrometer (gifts) on-board blackbody calibration system," *Proceedings of Society of Photographic Instrumentation Engineers (SPIE)*, vol. 5655, 2004.

[9] K. Hiraka, Y. Yamada, J. Ishii, H. Oikawa, T. Shimizu, S. Kadoya, and T. Kobayashi, "Compact fixed-point blackbody furnace with improved temperature uniformity and multi-fixed points use," in *Proceedings of SICE Annual Conference*, 2012, pp. 35–39.

[10] A. S. Sedra and K. C. Smith, *Microelectronic Circuits*, 6th ed. New York: Oxford University Press, 2010.

[11] A. Yariv, *Quantum Electronics*, 3rd ed. New York: John Wiley & Sons, 1988.

[12] Wikipedia, "Laser," Wikipedia, The Free Encyclopedia, Mar. 2013. [Online]. Available: http://en.wikipedia.org/w/index.php?title=Laser&oldid=544984333

[13] M. S. Bhatia and G. Kumar, "On the emi potential of various laser types," in *Proceedings of the International Conference on Electromagnetic Interference and Compatibility (INCEMIC)*, 2002, pp. 2–5.

[14] J. Faist, F. Capasso, D. L. Sivco, C. Sirtori, A. L. Hutchinson, and A. Y. Cho, "Quantum cascade laser," *Science*, vol. 264, pp. 553–556, 1994.

[15] R. Maulini, *Broadly Tunable Mid-infrared Quantum Cascade Lasers for Spectroscopic Applications*, Ph.D. dissertation, University of Neuchtel, Neuchtel, Switzerland, Dec. 2006.

[16] A. Hugi, R. Terrazi, Y. Bonetti, A. Whittmann, M. Fischer, M. Beck, J. Faist, and E. Gini, "External cavity quantum cascade laser tunable from 7.6 to 11.4 m," *Applied Physics Letters*, vol. 95, no. 6, pp. 061 103 – 061 103–3, Aug. 2009.

[17] L. Hvozdara, N. Pennington, M. Kraft, M. Karlowatz, and B. Mizaikoff, "Quantum cascade lasers for mid-infrared spectroscopy," *Vibrational Spectroscopy*, vol. 30, pp. 53–58, 2002.

[18] W. W. Bewly, J. R. Lindle, C. S. Kim, I. Vurgaftman, J. R. Meyer, A. J. Evans, J. S. Yu, S. Slivken, and M. Razeghi, "Beam steering in high-power cw qunatum-cascade lasers," *IEEE Journal of Quantum Electronics*, vol. 41, pp. 833–841, 2005.

[19] M. S. Taubman, "Transistor-based interface circuitry," U.S. Patent 7 176 755, Feb. 13, 2007.

[20] M. S. Taubman, "Current control circuitry," U.S. Patent 6 867 644, Mar. 15, 2005.

[21] M. S. Taubman, "Transistor-based interface circuitry," U.S. Patent 6 696 887, Feb. 24, 2004.

[22] M. S. Taubman, "Low-noise high-performance current contcontrol for quantum cascade lasers," *Review of Scientific Instruments*, vol. 82, no. 6, p. 8, 2011.

[23] Y. Zhang and J. Ashe, "Designing a high performance tec controller," *Proceedings of Society of Photographic Instrumentation Engineers, Semiconductor Lasers and Applications*, vol. 4913, p. 117, 2002.

[24] M. S. Taubman, T. L. Myers, R. M. Pratt, R. Stahl, and B. D. Cannon, "Precision control of multiple quantum cascade lasers for calibratoin systems," *Review of Scientific Instruments*, vol. 85, in press.

[25] J. R. Davis, Ed., *Copper and Copper Alloys*. Materials Park, OH: ASM International, 2001.

[26] A. Williams and F. J. Taylor, *Electronic Filter Design Handbook*, 4th ed., W. Rinaldi and J. McKenzie, Eds. New York: McGraw-Hill, 2006.

[27] *Ultra Precision Reference*, Linear Technology, datasheet LTZ1000/LTZ1000A.

[28] B. G. Rax, C. I. Lee, and A. H. Johnston, "Degradation of precision reference devices in space environments," *IEEE Transactions on Nuclear Science*, vol. 44, no. 6, pp. 1939–1944, Dec. 1997.

Appendices

Appendix A

Test Station

A.1 Test Station View 1

Figure A.1 shows the lab setup of the test station.

A.2 QCL Mount and Power Meter Head

Figure A.2 shows the QCL mount, Laser Power meter encased with a water jacket, and the commercial QCL current controller.

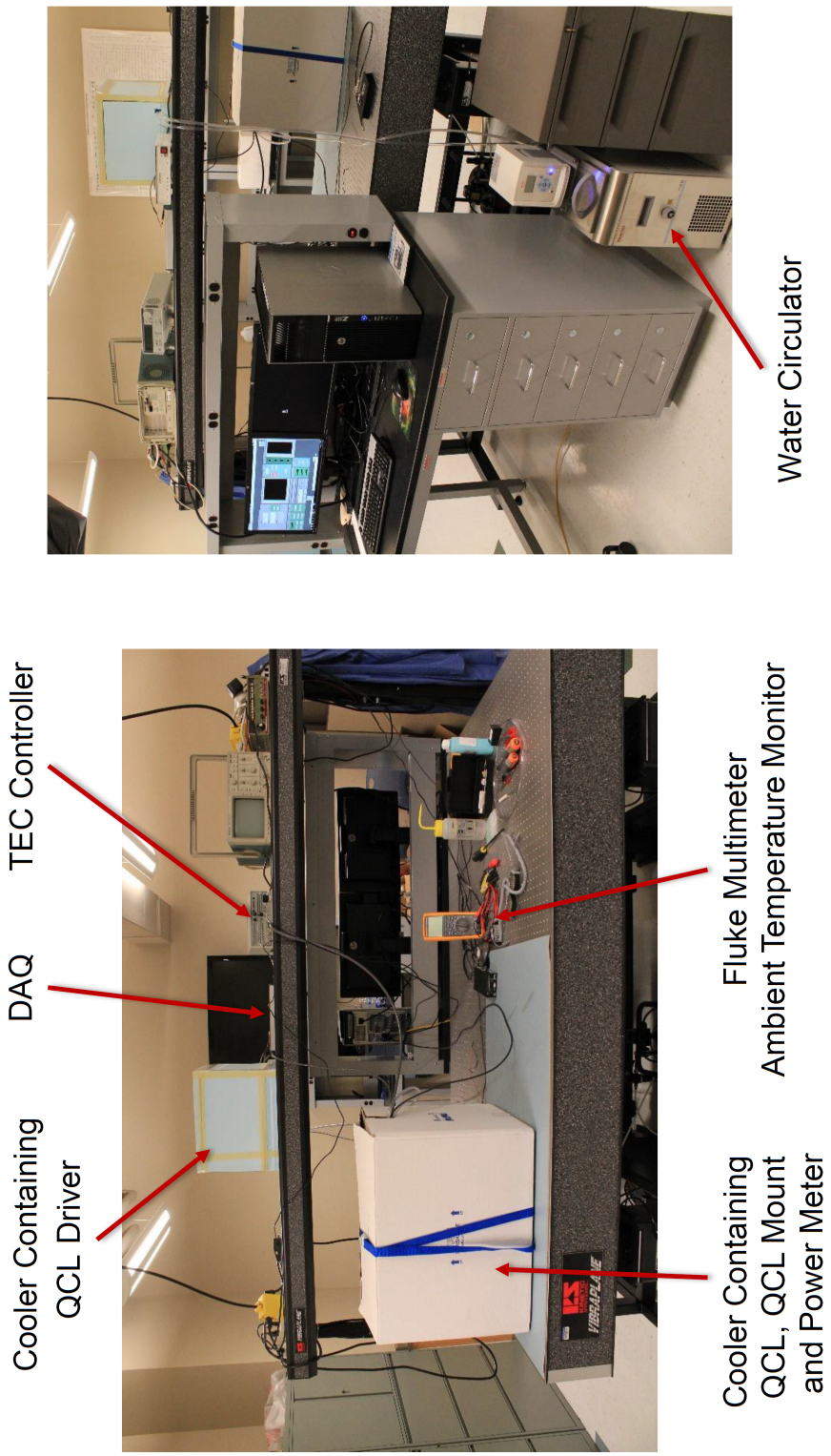

Fig. A.1: Test station.

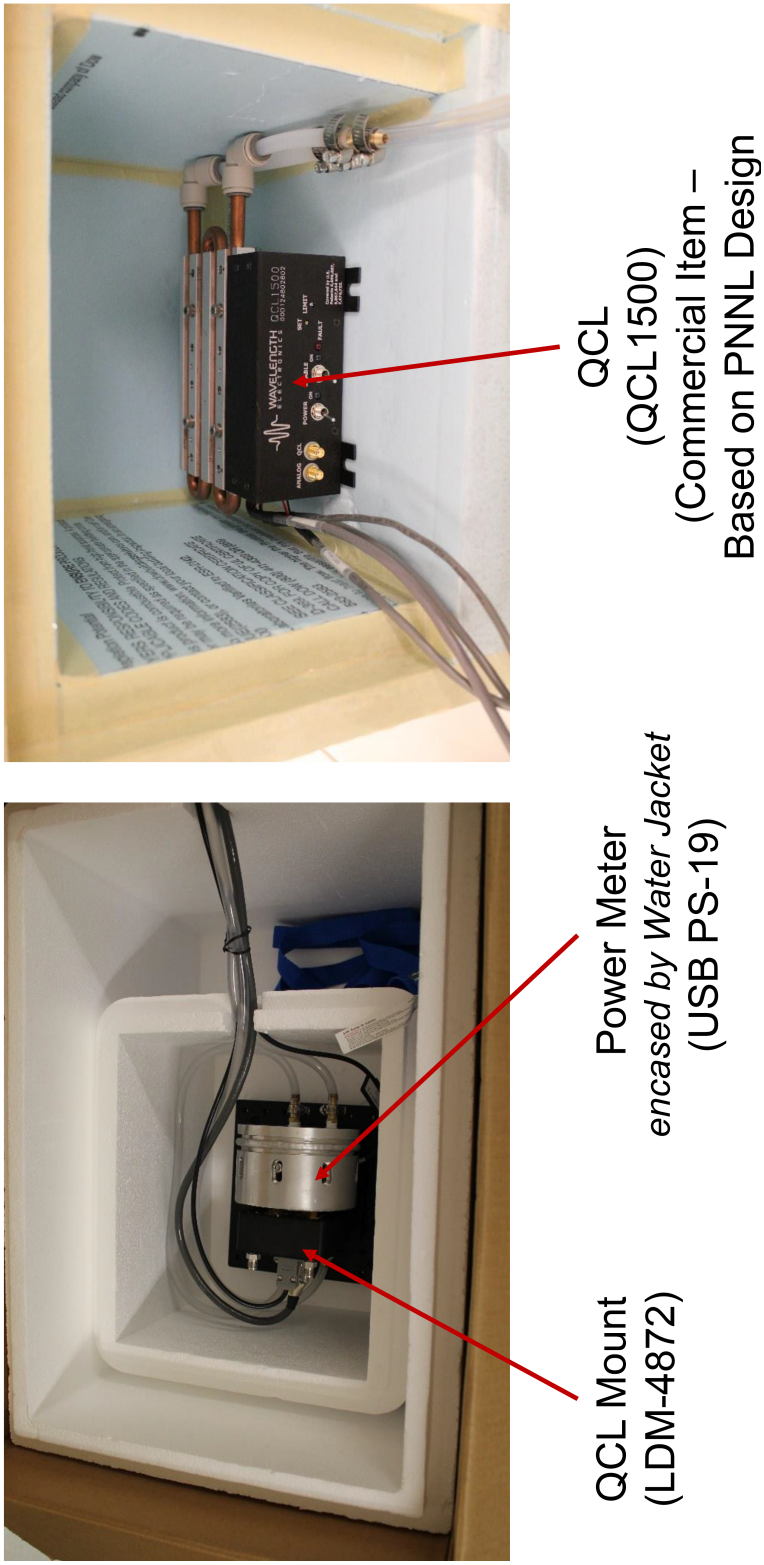

Fig. A.2: Cooler with QCL mount and power meter head with water jacket.

Appendix B

LabView

Figure B.1 shows the front panel of the LabView® program used to control the lab equipement for the QCL tests.

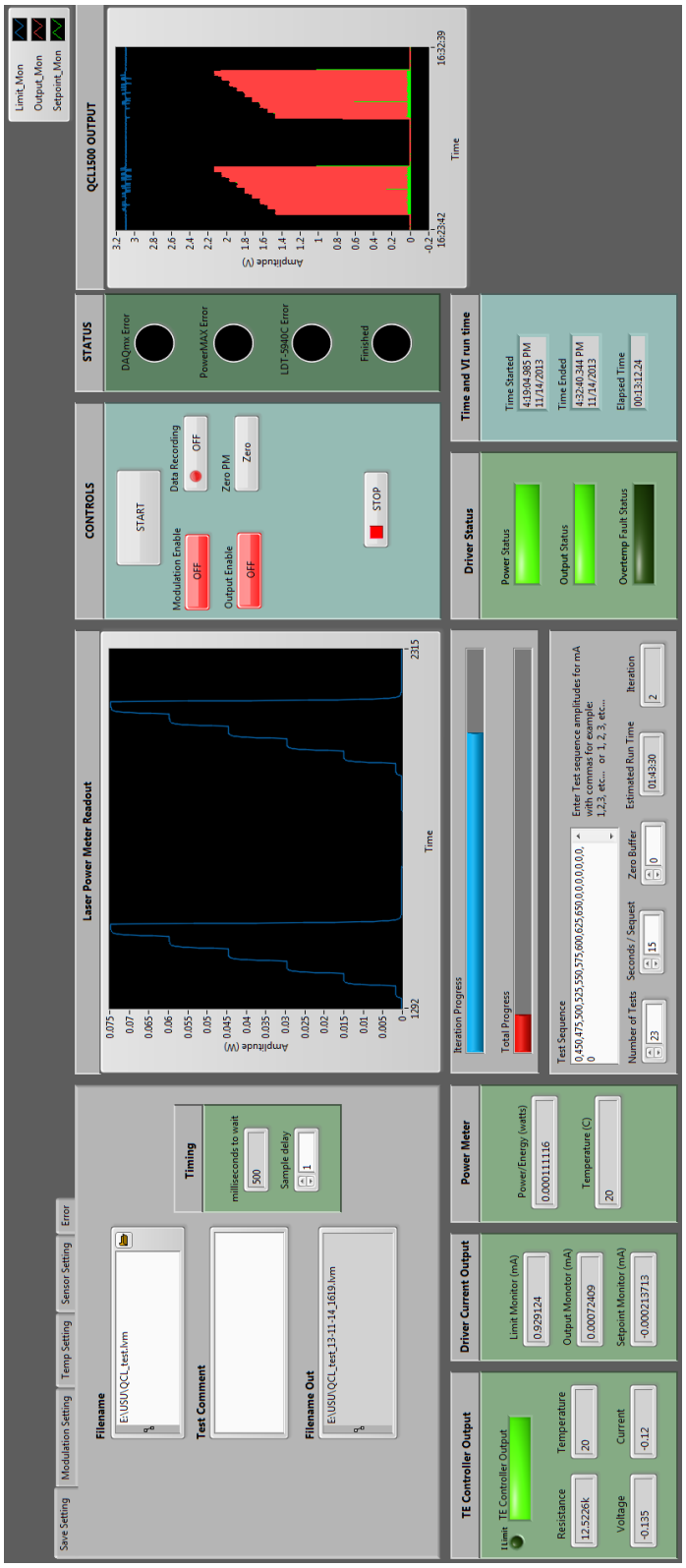

Fig. B.1: LabView front panel.

Appendix C

FPGA Simulations

This section reviews the simulation results. Figure C.1 shows a simulation with no errors in parity or communication. Figure C.2 shows a simulation with a parity error associated with FPGA response. Figure C.3 show the modulation frequency of 40 kHz. Figure C.4 shows a change in modulation frequency to 60 kHz. Figure C.5 show an overcurrent event and the result of the FPGA control.

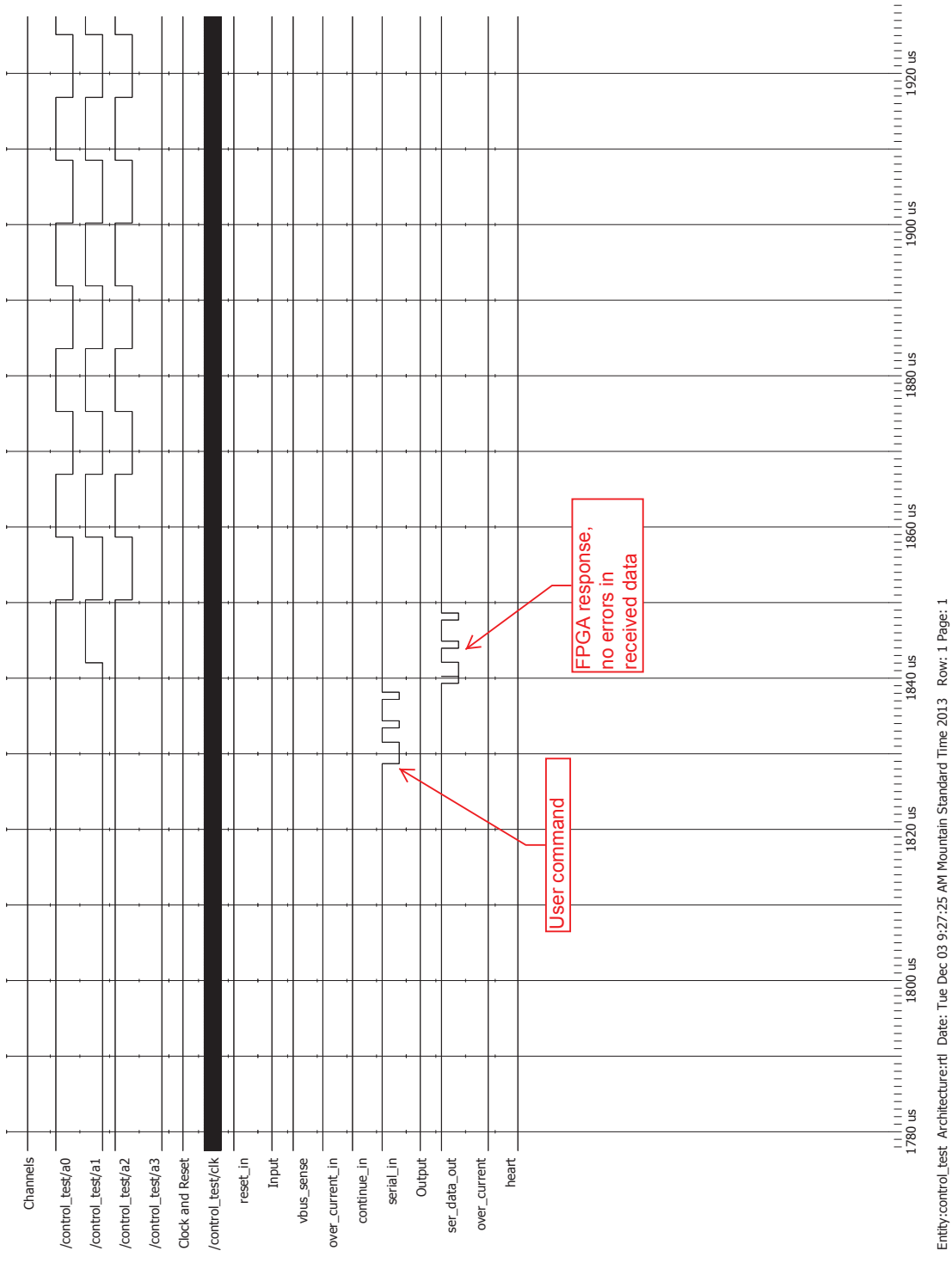

Fig. C.1: ACTEL simulation of the FPGA code with no error.

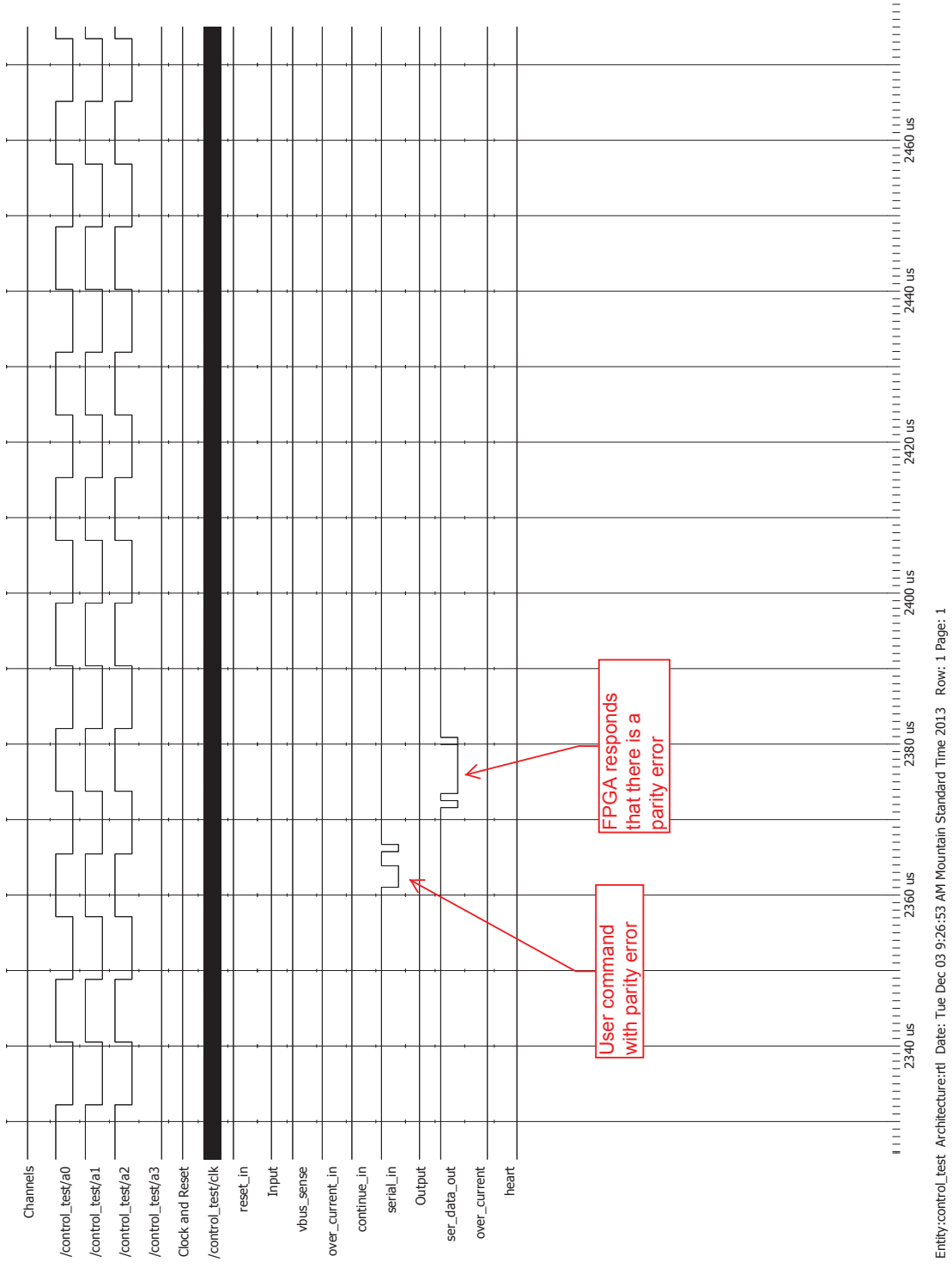

Fig. C.2: ACTEL simulation of the FPGA code with parity error.

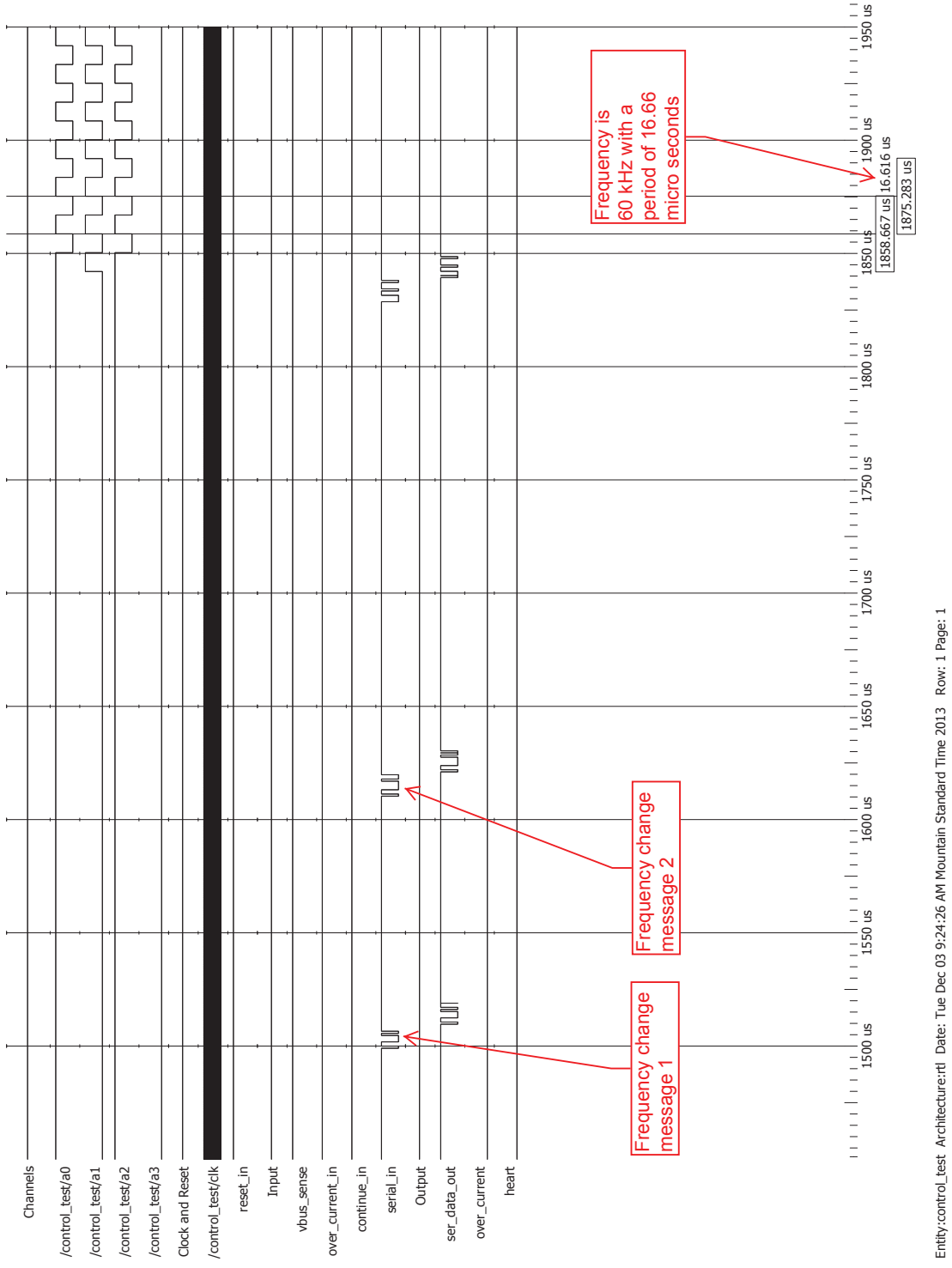

Fig. C.3: ACTEL simulation of the FPGA code with frequency change.

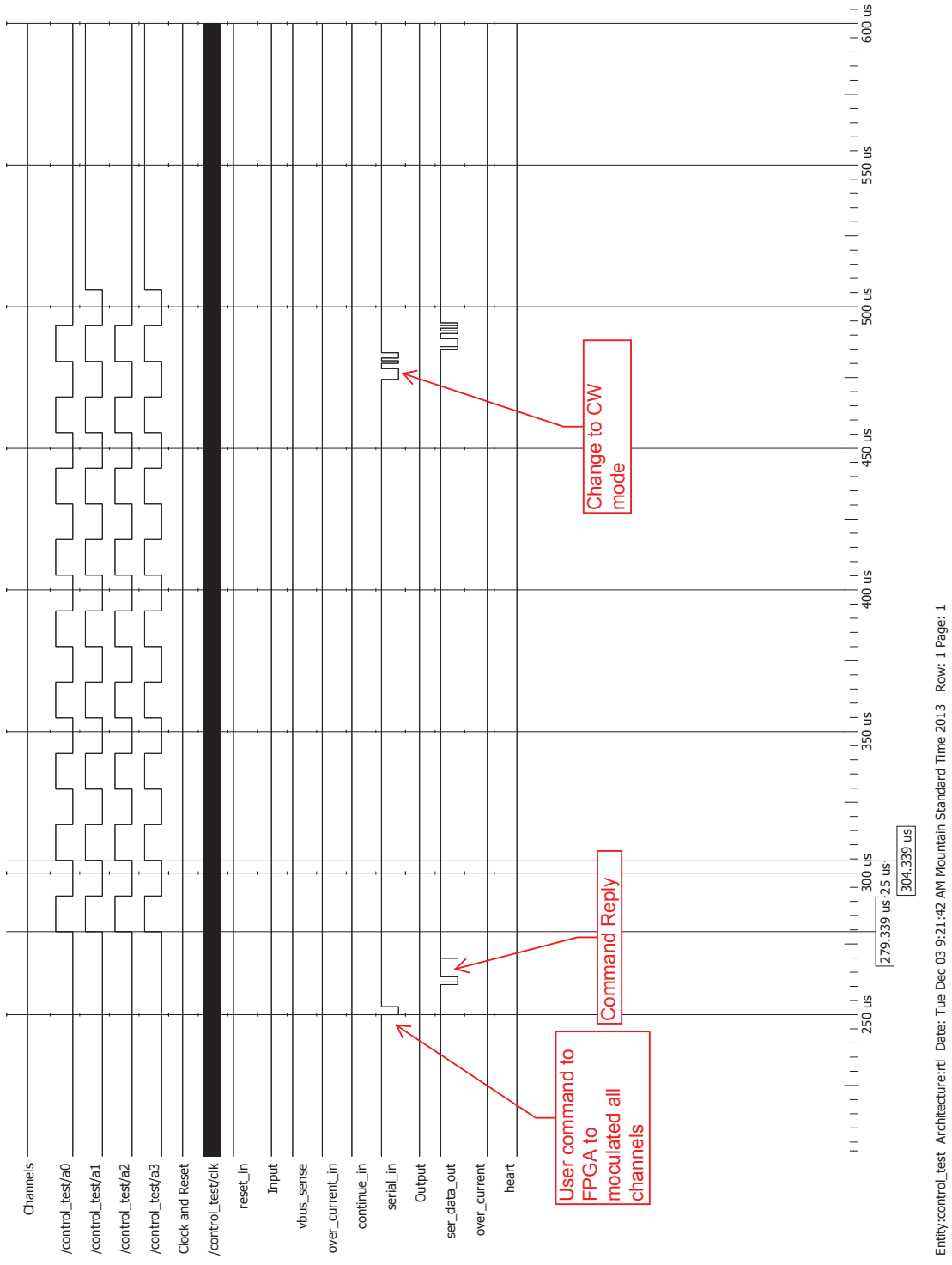

Fig. C.4: ACTEL simulation of the FPGA code with first and second.

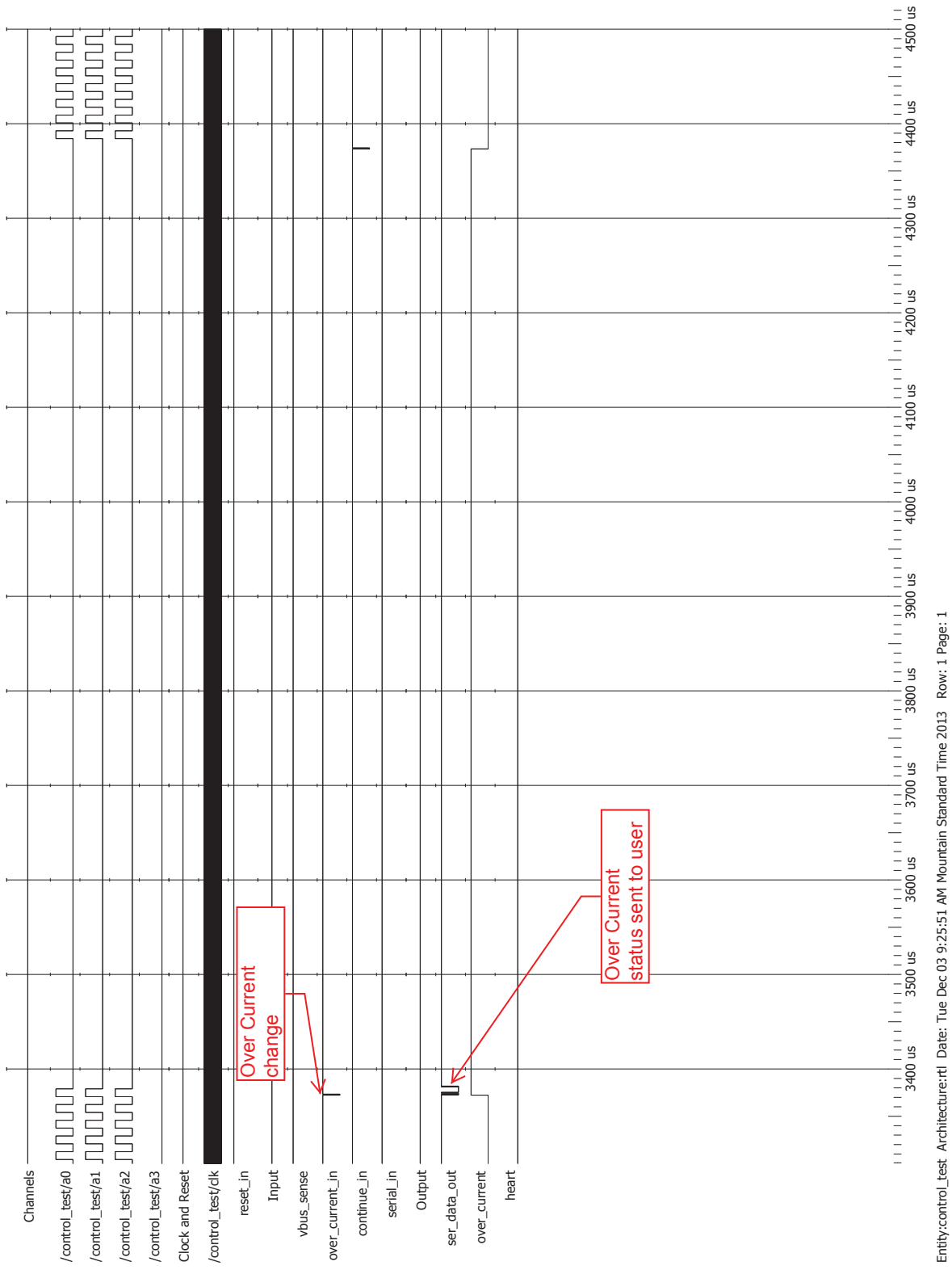

Fig. C.5: ACTEL simulation of the FPGA code overcurrent status change.

Appendix D

Electronics Simulations

D.1 Active Filter

D.2 Active Fitler Simulation Results

Using a capacitence multiplier design an active filter was designed to reduce the noise of the power rail inputs of sensitive devices. Simulation results for the active filter result are in Figure D.1.

D.3 Current Control Simulation

Figure D.2 shows the output voltages of the mux and voltage above the current sense resistor.

D.4 Current Control Noise Output

Figure D.3 displays the simulated output noise of the voltage of the current sense resistor.

Fig. D.1: Filter simulation results.

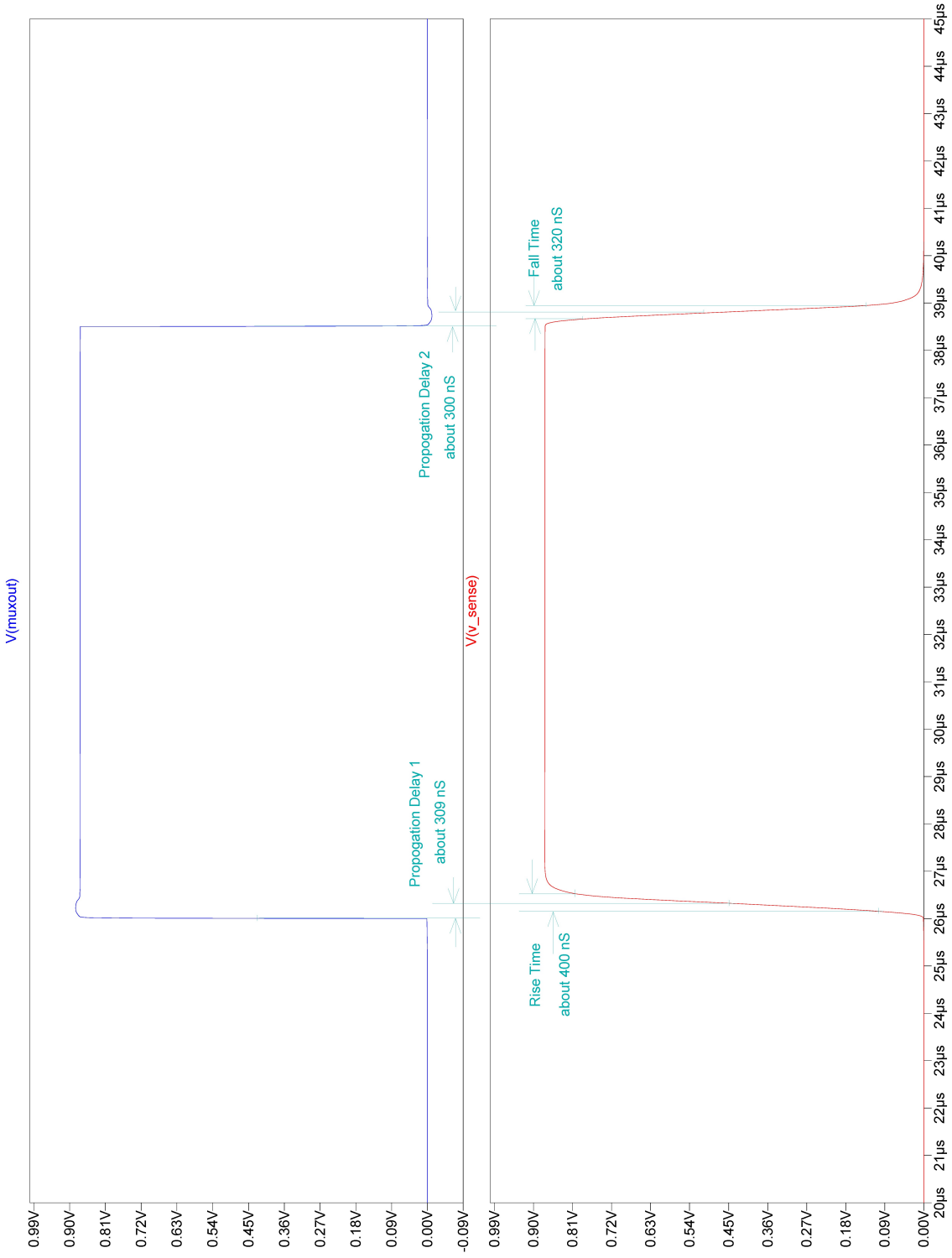

Fig. D.2: Current controller output.

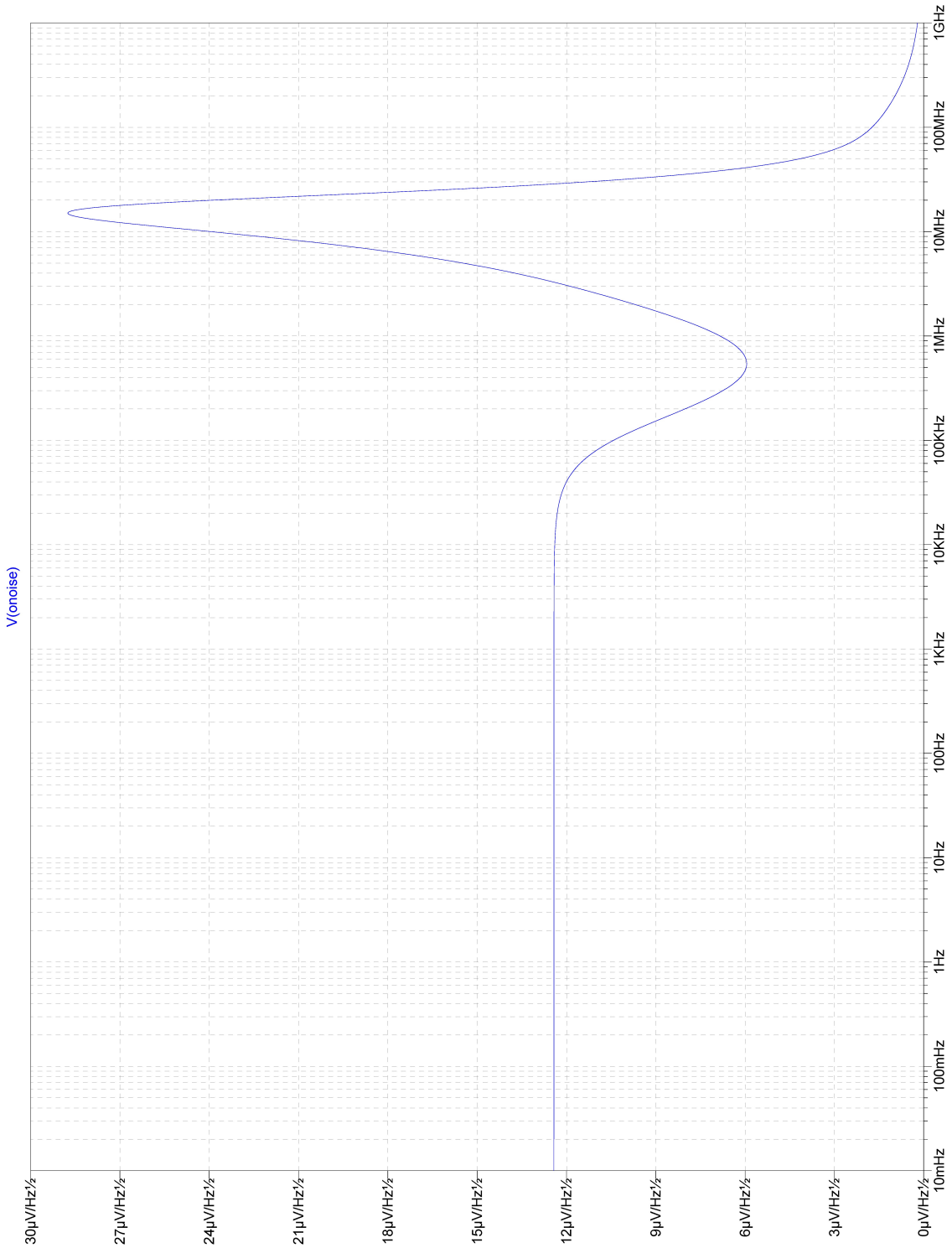

Fig. D.3: Current control noise output.